

ISBN: 978-1-68108-306-3
eISBN: 978-1-68108-305-6

ISSN: 2468-4716
eISSN: 2468-4724

FRONTIERS IN AEROSPACE SCIENCE

VOLUME 1

AEROSPACE STRUCTURES AND MATERIALS

Editor:
Yucheng Liu

Bentham  Books

Frontiers in Aerospace Science

Volume 1

Aerospace Structures and

Materials

Edited By

Yucheng Liu

Department of Mechanical Engineering

Mississippi State University

MS 39762

USA

Frontiers in Aerospace Science

Volume # 1

Aerospace Structures and Materials

Editor: Yucheng Liu

ISSN (Online): 2468-4724

ISSN: Print: 2468-4716

ISBN (eBook): 978-1-68108-305-6

ISBN (Print): 978-1-68108-306-3

© [2016], Bentham eBooks imprint.

Published by Bentham Science Publishers – Sharjah, UAE. All Rights Reserved.

BENTHAM SCIENCE PUBLISHERS LTD.

End User License Agreement (for non-institutional, personal use)

This is an agreement between you and Bentham Science Publishers Ltd. Please read this License Agreement carefully before using the ebook/echapter/ejournal (“**Work**”). Your use of the Work constitutes your agreement to the terms and conditions set forth in this License Agreement. If you do not agree to these terms and conditions then you should not use the Work.

Bentham Science Publishers agrees to grant you a non-exclusive, non-transferable limited license to use the Work subject to and in accordance with the following terms and conditions. This License Agreement is for non-library, personal use only. For a library / institutional / multi user license in respect of the Work, please contact: permission@benthamscience.org.

Usage Rules:

1. All rights reserved: The Work is the subject of copyright and Bentham Science Publishers either owns the Work (and the copyright in it) or is licensed to distribute the Work. You shall not copy, reproduce, modify, remove, delete, augment, add to, publish, transmit, sell, resell, create derivative works from, or in any way exploit the Work or make the Work available for others to do any of the same, in any form or by any means, in whole or in part, in each case without the prior written permission of Bentham Science Publishers, unless stated otherwise in this License Agreement.
2. You may download a copy of the Work on one occasion to one personal computer (including tablet, laptop, desktop, or other such devices). You may make one back-up copy of the Work to avoid losing it. The following DRM (Digital Rights Management) policy may also be applicable to the Work at Bentham Science Publishers’ election, acting in its sole discretion:
 - 25 ‘copy’ commands can be executed every 7 days in respect of the Work. The text selected for copying cannot extend to more than a single page. Each time a text ‘copy’ command is executed, irrespective of whether the text selection is made from within one page or from separate pages, it will be considered as a separate / individual ‘copy’ command.
 - 25 pages only from the Work can be printed every 7 days.
3. The unauthorised use or distribution of copyrighted or other proprietary content is illegal and could subject you to liability for substantial money damages. You will be liable for any damage resulting from your misuse of the Work or any violation of this License Agreement, including any infringement by you of copyrights or proprietary rights.

Disclaimer:

Bentham Science Publishers does not guarantee that the information in the Work is error-free, or warrant that it will meet your requirements or that access to the Work will be uninterrupted or error-free. The Work is provided "as is" without warranty of any kind, either express or implied or statutory, including, without limitation, implied warranties of merchantability and fitness for a particular purpose. The entire risk as to the results and performance of the Work is assumed by you. No responsibility is assumed by Bentham Science Publishers, its staff, editors and/or authors for any injury and/or damage to persons or property as a matter of products liability, negligence or otherwise, or from any use or operation of any methods, products instruction,

advertisements or ideas contained in the Work.

Limitation of Liability:

In no event will Bentham Science Publishers, its staff, editors and/or authors, be liable for any damages, including, without limitation, special, incidental and/or consequential damages and/or damages for lost data and/or profits arising out of (whether directly or indirectly) the use or inability to use the Work. The entire liability of Bentham Science Publishers shall be limited to the amount actually paid by you for the Work.

General:

1. Any dispute or claim arising out of or in connection with this License Agreement or the Work (including non-contractual disputes or claims) will be governed by and construed in accordance with the laws of the U.A.E. as applied in the Emirate of Dubai. Each party agrees that the courts of the Emirate of Dubai shall have exclusive jurisdiction to settle any dispute or claim arising out of or in connection with this License Agreement or the Work (including non-contractual disputes or claims).
2. Your rights under this License Agreement will automatically terminate without notice and without the need for a court order if at any point you breach any terms of this License Agreement. In no event will any delay or failure by Bentham Science Publishers in enforcing your compliance with this License Agreement constitute a waiver of any of its rights.
3. You acknowledge that you have read this License Agreement, and agree to be bound by its terms and conditions. To the extent that any other terms and conditions presented on any website of Bentham Science Publishers conflict with, or are inconsistent with, the terms and conditions set out in this License Agreement, you acknowledge that the terms and conditions set out in this License Agreement shall prevail.

Bentham Science Publishers Ltd.

Executive Suite Y - 2
PO Box 7917, Saif Zone
Sharjah, U.A.E.
Email: subscriptions@benthamscience.org



CONTENTS

PREFACE	i
LIST OF CONTRIBUTORS	ii
CHAPTER 1 ANALYSIS OF LINEAR/NON-LINEAR AEROELASTIC RESPONSE OF SUPERSONIC THICK FINS	3
<i>R.D. Firouz-Abadi, S.M. Alavi, M. Rahmanian and H. Haddadpour</i>	
NOMENCLATURE	4
INTRODUCTION	5
Linear Structural Modeling of a General Fin	9
Non-Linear Structural Modeling of 3D Fins	11
Aerodynamic Modeling of the Flexible Fins	14
Steady Supersonic Flow Over the Fin	15
Localized Piston Theory Including the Effects of Thickness and Angle of Attack	18
General Concepts in Nonlinear Analysis of Dynamical Systems	20
Bifurcation Theory	20
Phase Plots	21
Chaos	22
Lyapunov Exponents	22
Numerical Results	23
<i>Verification of Aerodynamic Model</i>	23
Effect of Thickness and Angle of Attack on the Aerodynamic Coefficient	25
Verification of Aeroelastic Model	26
Effect of Geometrical Parameters on the Aeroelastic Analysis	28
Aeroelastic Analysis of Elastic Fins	32
Non-linear Aeroelastic Analysis	35
Effects of Airspeed Mach Number	35
Effects of Thickness	40
Effect of Initial Angle of Attack	44
Effect of Hinge Position	47
Effect of Sweep Angle	51
Effect of Hinge Frictional Torque	55
CONFLICT OF INTEREST	61
ACKNOWLEDGEMENTS	62
NOTES	62
REFERENCES	62
CHAPTER 2 AN ANALYTICAL AND EXPERIMENTAL INVESTIGATION INTO VIBRATORY FORCE FOR AIRCRAFT WINGS	65
<i>Xueguang Bi and Yucheng Liu</i>	
INTRODUCTION	67
LITERATURE REVIEW	67
Analytical Study.....	67
Experimental Study.....	70
EVALUATE AERODYNAMIC FORCE USING 2DOF SYSTEM	71
2DOF Airfoil System.....	71
Force Determination Methods	74
<i>Traditional Force Determination Method</i>	74
<i>Force Determination Using "H1" & "H2" Estimated Frequency Response Matrices</i>	75
<i>Direct Force Determination "F1" and "F2" Methods</i>	76

Validation of Force Determination Methods	76
EVALUATE AERODYNAMICS FORCE USING MDOF SYSTEM	85
MDOF Aircraft Wing Model	85
Validation of Force Determination Methods	91
DISCUSSIONS	98
EXPERIMENT TESTINGS	98
Experiment Model	98
Ground Vibration Test	100
<i>Experiment Setup</i>	100
<i>Modal Analysis Methods</i>	102
<i>Results and Discussions</i>	103
Wind Tunnel Test	106
<i>Theoretical Background</i>	106
<i>Experiment Setup</i>	107
<i>Results and discussions</i>	108
CONCLUSION	109
CONFLICT OF INTEREST	109
ACKNOWLEDGEMENTS	109
REFERENCES	110

CHAPTER 3 COMPUTATIONAL AND ANALYTICAL INVESTIGATION OF LATERAL IMPACT BEHAVIOR OF PRESSURIZED PIPELINES	113
<i>Yangqing Dou and Yucheng Liu</i>	
NOMENCLATURE	114
INTRODUCTION	114
PROBLEM DESCRIPTION	116
MATERIAL PROPERTIES	117
COMPUTER MODELING AND ANALYSIS	118
COMPUTATIONAL IMPACT BEHAVIOR OF THE PIPELINE MODELS	121
FEA Results	121
Effects of Impact Position on the Impact Response of Pipelines	124
Effects of Internal Pressure on the Impact Response of Pipelines	130
DISCUSSION ON COMPUTER RESULTS	132
ANALYTICAL ANALYSIS	134
Response Surface Method (RSM)	134
RSM Models and Assessment	136
PARAMETRIC STUDY	141
Influence of Internal Pressure	141
INFLUENCE OF OUTSIDE DIAMETER	144
CONCLUSION	148
CONFLICT OF INTEREST	150
ACKNOWLEDGEMENTS	150
REFERENCES	150

CHAPTER 4 EFFECT OF BONDLINE THICKNESS ON THE TRACTION-SEPARATION LAWS OF ADHESIVELY BONDED JOINT	153
<i>Gefu Ji, Zhenyu Ouyang and Guoqiang Li</i>	
INTRODUCTION	154
Background	154
<i>Adhesive Bonding Technology</i>	154
Three Basic Modes of Fracture	155
Classical Fracture Mechanics	156
Nonlinear Fracture Mechanics	157

<i>Cohesive Zone Method</i>	157
J-Integral.....	157
Application of CZM in Adhesive Joint.....	158
Effects of Adhesive Thickness.....	162
Research Objectives	163
THEORETICAL BACKGROUND	164
Theoretical Derivations	165
Governing Equations	168
J- Integral for Interface Shear Behaviors	169
J- Integral for Interface Peel Behaviors	171
Determination of Interface Cohesive Laws	172
Fracture Tests by DCB, ENF and SLB Specimens	173
DCB Specimens for Mode-I Fracture Test	174
ENF Specimens for Mode-II Fracture Test	175
SLB Specimens for Mixed Mode I/II Fracture Test	177
EXPERIMENTAL METHOD	180
Raw Material	180
<i>Adhesive Material</i>	180
<i>Adherends Material</i>	181
Fabrication of Specimen	181
Steel Based DCB Specimen for Mode I Test	182
Steel Based ENF Specimen for Mode II Test	183
Steel Based Single Leg Bending Specimen for Mixed Mode I/II Test	184
Fabrication of Self-Aligned Ball Pin	185
Instrumentation and Test Method	186
RESULTS AND DISCUSSION OF MODE I TEST	189
Results and Discussions of Mode I Test	189
<i>Global Test Results</i>	189
<i>Local Test Results</i>	192
Effects of the Thickness of the Adhesive Layer	194
RESULTS AND DISCUSSIONS OF MODE II TEST	200
Global and Local Experimental Results	200
Effects of the Thickness of the Adhesive Layer	204
RESULTS AND DISCUSSION OF MIXED MODE I AND MODE II TEST	209
Global and Local Test Results	209
Effects of the Thickness of the Adhesive Layer	215
<i>Mode I Portion</i>	216
<i>Mode II Portion</i>	218
<i>Mode Mixities</i>	219
Effects of the Initial Crack Tip Length of the Adhesive Layer	221
CONCLUSIONS AND FUTURE WORKS	228
Mode I Test	228
Mode II Test	229
Mixed Mode I/II Test	230
CONFLICT OF INTEREST	231
ACKNOWLEDGEMENTS	231
REFERENCE	231
CHAPTER 5 OPTIMIZATION OF GEOMETRIC PARAMETERS AND REVERSING DESIGN	
METHODOLOGY OF INVESTMENT CASTING DIE PROFILE OF TURBINE BLADE	240
<i>Yangqing Dou, Yangliu Dou, Kun Bu and Yiwei Dong</i>	
NOMENCLATURE	241

INTRODUCTION	242
OPTIMIZATION OF GEOMETRIC PARAMETERS FOR TURBINE BLADE	244
Geometric Parameter Extraction of Cross-section.....	244
Extraction of Bending Control Parameters.....	245
Extraction of Torsional Control Parameters.....	247
Optimization of Torsional Control Parameters.....	247
Optimization of Bending Control Parameters.....	247
Results and Discussion.....	251
OPTIMUM DESIGN METHOD OF DIE PROFILE	254
ANALYSIS OF FILES GENERATED DURING NUMERICAL SIMULATION PROCESS	256
FEM PROCESSING	257
EXAMPLE VERIFICATION	260
CONCLUSION	265
CONFLICT OF INTEREST	266
ACKNOWLEDGEMENTS	266
REFERENCES	266
CHAPTER 6 VIBRATION INDUCED FATIGUE ANALYSIS OF AEROSPACE STRUCTURES	269
<i>Murat Aykan and Mehmet Çelik</i>	
INTRODUCTION	270
FLIGHT TESTS AND NUMERICAL ANALYSES OF AN ANTENNA FOR SAFETY OF FLIGHT	
.....	273
Operational Flight Tests before Integration	273
Numerical Structural Analyses.....	273
Operational Flight Tests After Integration.....	277
VIBRATION INDUCED FATIGUE ANALYSIS AND TESTING OF A CHAFF/FLARE DISPENSER	
BRACKET	279
Vibration Fatigue Analysis Method.....	281
Fatigue Analysis and Tests	286
<i>Analysis of Design-1</i>	290
<i>Analysis of Design-2</i>	292
<i>Analysis of Design-3</i>	294
CONCLUSION	297
CONFLICT OF INTEREST	299
ACKNOWLEDGEMENTS	299
REFERENCES	299
CHAPTER 7 FATIGUE LIFE OPTIMIZATION OF LASER PEENED AIRCRAFT COMPONENTS	302
<i>Anoop Vasu and Ramana V. Grandhi</i>	
NOMENCLATURE	303
INTRODUCTION	303
INFLUENCING FACTORS FOR FATIGUE LIFE PREDICTION	308
Applied Load.....	309
Laser Peening Induced Residual Stresses	310
Residual Stress Relaxation.....	311
Fatigue Life.....	312
Re-Peening.....	314
OPTIMIZATION PROCEDURE	314
Design Variables.....	315
<i>Re-Peening Schedule</i>	315
<i>Mid-Span Duration</i>	316
<i>Peak Pressure</i>	317
<i>Percentage Overlap</i>	317

Optimization strategy	319
RESULTS AND DISCUSSION	320
Compressive Residual Stress Optimization Results	320
Optimization of the Re-Peening Schedule	322
CONCLUSION	323
CONFLICT OF INTEREST	324
ACKNOWLEDGEMENTS	324
REFERENCES	324

CHAPTER 8 PREDICTION OF RESIDUAL STRESS RELAXATION IN TI-6AL-4V SUBJECTED TO LASER PEENING 327

<i>Anoop Vasu and Ramana V. Grandhi</i>	
NOMENCLATURE	328
INTRODUCTION	329
LASER PEENING MECHANISM	332
Pressure Pulse Generation	333
High Strain Rate Phenomenon	334
Plasticity in Laser Peening	335
FINITE ELEMENT MODELING OF LASER PEENING	336
Pressure Pulse Input	337
Simulation Procedure	337
Constitutive Model	339
Effect of Temperature in Laser Peening Process	339
Curvature Effect	342
RESIDUAL STRESS RELAXATION	344
Obtain Empirical Data for Calibration	346
FE Modeling of Stress Relaxation	347
RESULTS AND DISCUSSION	348
CONCLUSION	350
CONFLICT OF INTEREST	351
ACKNOWLEDGEMENTS	351
REFERENCES	351

CHAPTER 9 NON-DESTRUCTIVE EVALUATION (NDE) OF WELDED STRUCTURES FOR AEROSPACE APPLICATIONS 355

<i>Mohammad W. Dewan, Daniel J. Huggett and Muhammad A. Wahab</i>	
INTRODUCTION	356
ULTRASONIC TESTING (UT)	358
FUNDAMENTALS OF ULTRASONIC TESTING	359
CONVENTIONAL ULTRASONIC TESTING (UT)	364
TIME-OF-FLIGHT-DIFFRACTION (TOFD) ULTRASONIC TESTING	366
PHASED ARRAY ULTRASONIC TESTING (PAUT)	369
Defect Sizing Using PAUT	373
Case Study: Welding Defect Detection with PAUT	376
RADIOGRAPHIC TESTING (RT)	378
FUNDAMENTALS OF RADIOGRAPHIC TESTING	379
Case study: Welding Defect Detection with RT	385
Comparison of PAUT and RT to obtain Welding Defect	386
CONCLUSION	387
CONFLICT OF INTEREST	388
ACKNOWLEDGEMENTS	388
REFERENCES	388

CHAPTER 10	DEVELOPMENT OF A REMOTELY PILOTED HELICOPTER FOR CIVIL APPLICATIONS	393
	<i>N. Goudarzi, R. M. Ziazi, F. Kermanshahi, S. Sadati, M. S. Sajedi and M. Mohaghegh</i>	
	NOMENCLATURE	394
	INTRODUCTION	396
	CONCEPTUAL DESIGN	397
	2.1. Weight Sizing	398
	2.2. Configuration Selection	399
	2.3. Rotor Sizing	400
	2.4. Aerodynamic Sizing	402
	2.5. Power Sizing	402
	DETAILED DESIGN	403
	3.1. Engine and Fuel System	404
	3.2. Blade Selection	408
	3.3. Power Transmitting System	409
	STABILITY AND CONTROL OF A REMOTELY PILOTED HELICOPTER	412
	4.1. Dynamic Modeling	414
	4.1.1. Methodology	414
	4.1.2. Rigid Body Equations of Motion	418
	4.2. Trim and Stability Analysis	420
	4.2.1. Analysis of the Trim	420
	4.2.2. Stability	421
	CATIA MODELING	427
	MANUFACTURING AND ASSEMBLING	428
	TEST AND RELIABILITY ANALYSIS	430
	CONCLUSION	437
	CONFLICT OF INTEREST	437
	ACKNOWLEDGEMENTS	438
	REFERENCES	438
CHAPTER 11	MATERIALS SELECTION IN DESIGN OF STRUCTURES OF SUBSONIC AND SUPERSONIC AIRCRAFTS	442
	<i>Zainul Huda</i>	
	NOMENCLATURE	443
	INTRODUCTION	443
	OPERATING CONDITIONS AND MATERIAL SELECTION	445
	Environmental Service Conditions	445
	Loading Conditions and Design Relationships	447
	<i>Design Equation for Tension</i>	447
	<i>Design Equation for Compression</i>	448
	<i>Design Equation for Bending</i>	448
	<i>Design Equation for Torsion</i>	448
	Materials Selection for Aircraft Structure --- A Design Approach	449
	MATERIALS SELECTION BASED ON SPEED AND TEMPERATURE	451
	Materials Selection for Subsonic Structures (for Speeds ≤ 1.0 Mach)	451
	Materials Selection for Structures with Speeds ≤ 2.0 Mach	454
	Materials Selection for Structure for Speeds Between 2.0 and 4.0 Mach	456
	Material-Selection for Military Aircraft Wings	460
	A NEW MATERIALS SELECTION CHART FOR SSTAS	462
	CONCLUSIONS AND RECOMMENDATIONS	463
	CONFLICT OF INTEREST	463
	ACKNOWLEDGEMENTS	464

REFERENCES	464
CHAPTER 12 POTENTIAL AEROSPACE APPLICATIONS OF CARBON NANOTUBES	468
<i>Omid Gohardani</i>	
NOMENCLATURE	469
INTRODUCTION	469
CARBON NANOTUBES IN AEROSPACE - HISTORICAL OVERVIEW	471
CARBON NANOTUBES IN AERONAUTICS	474
Recent Studies	479
CARBON NANOTUBES AND UNMANNED AERIAL VEHICLES	480
Recent Studies	481
CARBON NANOTUBES IN ASTRONAUTICS	481
Recent Studies	482
CHALLENGES RELATED TO CARBON NANOTUBE USAGE IN AEROSPACE SCIENCES	482
DISCUSSION AND FUTURE OUTLOOKS	485
CONFLICT OF INTEREST	486
ACKNOWLEDGMENTS	486
REFERENCES	486
CHAPTER 13 COMBINATION OF CARBON FIBER SHEET MOLDING COMPOUND AND PRE-IMPREGNATED, TAILORED CARBON FIBER REINFORCEMENTS	497
<i>Marc Fette, Nicole Stöß, Jens Wulfsberg, Axel Herrmann, Gerhard Ziegmann and Georg Lonsdorfer</i>	
NOMENCLATURE	498
INTRODUCTION	498
STATE OF THE ART	500
AIM AND PURPOSE OF THE PRESENT WORK	501
Experimental Procedures	504
DISCUSSION ON RESULTS	508
CONCLUSION	512
CONFLICT OF INTEREST	512
ACKNOWLEDGEMENTS	513
REFERENCES	513
CHAPTER 14 DESIGN OPTIMIZATION OF VARIABLE STIFFNESS COMPOSITE STRUCTURES FOR AEROSPACE APPLICATIONS	515
<i>Mohammad Rouhi, Hossein Ghayoor, Suong V. Hoa and Mehdi Hojjati</i>	
INTRODUCTION	516
MODELING AND ANALYSIS	519
DESIGN OPTIMIZATION	522
RESULTS	524
4.1. Bending-Induced Buckling of a Circular Cylinder	524
4.1.1. Effect of the Aspect Ratio (L/R)	526
4.1.2. Effect of the Radius (R)	528
4.1.3. Effect of the Steered Plies Percentage	529
4.2. Multi-Objective Design Optimization for Bending-Induced Buckling	530
4.3. Axial Buckling of an Elliptical Cylinder	532
CONCLUSION	535
CONFLICT OF INTEREST	535
ACKNOWLEDGEMENTS	535
REFERENCES	535
CHAPTER 15 MANUFACTURING CHALLENGES ASSOCIATED WITH THE USE OF METAL MATRIX COMPOSITES IN AEROSPACE STRUCTURES	542
<i>Tracie Prater</i>	
NOMENCLATURE	543

INTRODUCTION	544
PROBLEM DESCRIPTION	547
RELATIONSHIP BETWEEN WEAR AND PROCESS PARAMETERS	548
CONSTRUCTING AN ANALYTICAL MODEL OF THE WEAR PROCESS	551
COMBATTING WEAR: SELECTION OF TOOL MATERIALS	557
<i>IN SITU</i> SENSING OF WEAR USING TORQUE	558
CONCLUSION	559
CONFLICT OF INTEREST	561
ACKNOWLEDGEMENTS	561
REFERENCES	561
SUBJECT INDEX	564

PREFACE

This book covers a variety of aspects of design, analysis, and manufacturing of aerospace structures and materials, which include design/failure criteria for aerospace structures, materials selection, manufacturing methods, engineering design and analysis of structural assemblies and components, concurrent engineering, and interdisciplinary design technology.

Challenges that current aerospace engineers are faced with are as follows. First, they must understand the new and existing materials and the level of engineering already applied in their creation. Second, they need to develop a working design by combining material behavior and structural function to meet all the design requirements. Third, an optimum design has to be conducted based on the original working design to address manufacturability and economical constraints. Finally, the durability and longevity of the final structure should be continually assessed.

This book equips aerospace engineers with the necessary knowledge and practical skills to tackle these challenges in an industrial or R&D environment. Readers of this book will acquire knowledge of a broad range of the entire process in the context of the design, manufacturing, and analysis of aerospace structures and components. The readers will also be exposed to advanced research and development in fields directly relevant to aerospace engineering, which will improve our capability to design the next generation of aerospace structures and materials.

Interesting topics that will be demonstrated through this book include: structural dynamics and impact simulation, acoustic and vibration testing and analysis, fatigue analysis and life optimization, reversing design methodology, non-destructive evaluation, remotely piloted helicopter, surface enhancement of aerospace alloys, manufacturing of metal matrix composites, aerospace applications of carbon nanotubes, carbon fiber reinforcements, variable stiffness composites, aircraft material selection, *etc.* Furthermore, besides aerospace engineering, the topics included in this book also impact a broad variety of engineering areas such as mechanical engineering, materials engineering and science, civil engineering, automotive engineering, computer engineering and science, *etc.*

The book is intended to serve as a reference for researchers, engineers, engineering faculty, as well as graduate students. Finally, the editor would like to extend cordial appreciation to all contributors for their great support and invaluable contributions.

Yucheng Liu
Department of Mechanical Engineering
Mississippi State University
MS 39762, USA

List of Contributors

Anoop Vasu	Department of Mechanical and Materials Engineering, Wright State University, Dayton, USA
Axel Herrmann	Composite Technology Center GmbH (An Airbus Company), Stade, Germany
Daniel J. Huggett	Department of Mechanical and Industrial Engineering, Louisiana State University, Baton Rouge, USA
F. Kermanshahi	Ecole Polytechnique de Montreal, Quebec, Canada
Gefu Ji	Department of Mechanical & Industrial Engineering, Louisiana State University, Baton Rouge, USA
Georg Lonsdorfer	Composite Technology Center GmbH (An Airbus Company), Stade, Germany
Gerhard Ziegmann	Institute of Polymer Materials and Plastics Engineering, TU Clausthal, Clausthal, Germany
Guoqiang Li	Department of Mechanical & Industrial Engineering, Louisiana State University, Baton Rouge, USA Department of Mechanical Engineering, Southern University, Baton Rouge, USA
Hossein Ghayoor	Concordia Center for Composites, Department of Mechanical and Industrial Engineering, Concordia University, Montreal, Canada
H. Haddadpour	Department of Aerospace Engineering, Sharif University of Technology, Tehran, Iran
Jens Wulfsberg	Institute of Production Engineering, Helmut Schmidt University, Hamburg, Germany.
Kun Bu	Department of Mechanical Engineering, Mississippi State University, USA
Marc Fette	Institute of Production Engineering, Helmut Schmidt University, Hamburg, Germany. Composite Technology Center GmbH (An Airbus Company), Stade, Germany
Mehdi Hojjati	Concordia Center for Composites, Department of Mechanical and Industrial Engineering, Concordia University, Montreal, Canada
Mehmet Çelik	Department of Mechanical Engineering, SST Division-ASELSAN Inc., Turkey
Mohammad Rouhi	Concordia Center for Composites, Department of Mechanical and Industrial Engineering, Concordia University, Montreal, Canada
Mohammad W. Dewan	Department of Mechanical and Industrial Engineering, Louisiana State University, Baton Rouge, USA

Muhammad A. Wahab	Department of Mechanical and Industrial Engineering, Louisiana State University, Baton Rouge, USA
Murat Aykan	Department of Mechanical Engineering, MGEO Division-ASELSAN Inc., Turkey
M. Mohagheghi	Aerospace Engineering Department, University of Tehran, Tehran, Iran
M. Rahmanian	Department of Aerospace Engineering, Sharif University of Technology, Tehran, Iran
M. S. Sajedi	Aerospace Engineering Department, Amirkabir University of Technology, Tehran, Iran
Nicole Stöb	Polynt Composites Germany GmbH, Kieselstraße, Miehlen, Germany
N. Goudarzi	Mechanical Engineering Department, University of Maryland, USA
Omid Gohardani	Springs of Dreams Corporation, Tustin, USA
Ramana V. Grandhi	Department of Mechanical and Materials Engineering, Wright State University, Dayton, USA
R.D. Firouz-abadi	Department of Aerospace Engineering, Sharif University of Technology, Tehran, Iran
R. M. Ziazi	School of Mechanical, Industrial, and Manufacturing Engineering, Oregon State University, USA
Suong V. Hoa	Concordia Center for Composites, Department of Mechanical and Industrial Engineering, Concordia University, Montreal, Canada
S.M. Alavi	Department of Aerospace Engineering, Sharif University of Technology, Tehran, Iran
S. Sadati	Sustainable Environment and Energy Systems Department, Middle East Technical University, Northern Cyprus Campus
Tracie Prater	NASA Marshall SpaceFlight Center, Huntsville, USA
Xueguang Bi	Department of Mechanical Engineering, Mississippi State University, USA
Yangliu Dou	Department of Mechanical Engineering, Mississippi State University, USA
Yangqing Dou	Department of Mechanical Engineering, Mississippi State University, USA
Yiwei Dong	Department of Mechanical Engineering, Mississippi State University, USA
Yucheng Liu	Department of Mechanical Engineering, Mississippi State University, USA
Zainul Huda	Department of Mechanical Engineering, King Abdulaziz University, Jeddah, Saudi Arabia
Zhenyu Ouyang	Department of Mechanical & Industrial Engineering, Louisiana State University, Baton Rouge, USA

CHAPTER 1

Analysis of Linear/Non-Linear Aeroelastic Response of Supersonic Thick Fins**R.D. Firouz-Abadi^{*}, S.M. Alavi, M. Rahmanian and H. Haddadpour***Department of Aerospace Engineering, Sharif University of Technology, Tehran, P.O.Box 11115-8639, Iran*

Abstract: This study introduces an aeroelastic model for the linear/non-linear analysis of thick fins in supersonic or hypersonic regimes. In the first step a linear aeroelastic model for the analysis of thick fins is developed. To this aim, a thick fin with two degrees of freedom (2 DOF) as well as an elastic double-wedged fin in supersonic/hypersonic flight regimes are considered. An unsteady aerodynamic model is developed based on the shock/expansion theory by local application of the piston theory over the flat surfaces of the fin. The structural model is also obtained based on the Lagrangian approach. Employing such developed model, the effects of initial angle of attack, thickness and some other geometrical parameters on the aeroelastic stability boundaries and unsteady aerodynamic loads are studied. In the next step, a more sophisticated model describing the non-linear aeroelastic behavior of fins with 3 DOF and free-plays in flapping, plunging and pitching motions is investigated. To this aim, governing equations are obtained by a modification of the linear model and effects of several geometrical parameters (*e.g.* thickness, initial angle of attack, hinge frictional torque *etc.*) on the aeroelastic behavior of fins are assessed¹.

***Corresponding author R.D. Firouz-abadi:** Department of Aerospace Engineering, Sharif University of Technology, Tehran, P.O.Box 11115-8639, Iran; Tel: (+9821) 66164606; Fax: (+9821) 66022731; E-mail: firouzabadi@sharif.edu.

Keywords: Aeroelasticity, Free-play, Local piston theory, Shock and expansion analysis, Thick supersonic fin.

NOMENCLATURE

C_α, C_β, C_h	Structural damping.
\mathbf{C}^α	Aerodynamic damping matrix.
\mathbf{C}_s	Structural damping matrix.
D	Rayleigh dissipation function.
\mathbf{e}	Elastic displacement vector.
$\bar{\mathbf{e}}$	Natural mode shapes of the elastic displacements.
\mathbf{f}	Generalized forces.
h	Plunging displacement.
$\bar{I}_{xx}, \bar{I}_{xz}, \bar{I}_{zz}$	Mass moment of inertia
K_α, K_β, K_h	Spring Stiffness.
\mathbf{K}^α	Aerodynamic stiffness matrix.
KE	Kinetic energy.
\mathbf{K}_s	Structural stiffness matrix.
L_α	Lift.
m	Fin mass.
M	Mach number.
M_α	Flapping moment.
\mathbf{M}_s	Structural mass matrix.
\mathbf{n}	Outward unit normal of the undeformed surface.
p	Pressure.
P	Potential energy.
q	ith generalized coordinate.
Q_i	ith generalized forces.

S_α, S_β	Static mass moment of the fin about the elastic axis.
T	Temperature.
T_α	Pitching moment.
u	Flow velocity.
\mathbf{v}	Unit direction vector of the air velocity.
w	Displacements along the normal vector of each surface.
\mathbf{x}	Vector of dynamic states.
\bar{x}, \bar{z}	Position of the center of gravity related to elastic axis.
α	Pitch angle.
β	Flap angle.
α_f, β_f, h_f	Free-plays of the corresponding degrees of freedom.
γ	Specific heat ratio.
v	Prandtl-Meyer function.
θ	Elastic rotation vector.
$\bar{\theta}$	Natural mode shapes of the elastic rotations.
ρ	Density.
ω	Natural frequency.
ψ	Oblique wave angle.
ξ	Generalized modal coordinates.

INTRODUCTION

Commonly, an aeroelastic problem has two types of modeling including aerodynamic loads and structural response calculation. Combination of these two types of modeling yields a coupled fluid-structure system which may be unstable in some flight conditions. In the present chapter, aeroelastic response of fins in supersonic/hypersonic flow is aimed. This matter leads to centralize on the unsteady aerodynamic loading models in supersonic/hypersonic regimes. One of the most applied unsteady

CHAPTER 2

An Analytical and Experimental Investigation into Vibratory Force for Aircraft Wings

Xueguang Bi and Yucheng Liu*

Department of Mechanical Engineering, Mississippi State University, MS 39762, USA

Abstract: This paper focus on the assessment of aerodynamic forces applied on an aircraft. First, numerical analysis is performed on a simplified linear two-degree-of-freedom (2DOF) airfoil system model. Methods of aerodynamic force determination are established at different airspeed conditions and the calculated dynamic forces correlated well to the actual forces. Next, a finite element model of the airfoil is developed to represent its structural dynamics, and the established force determination methods are applied to determine the aerodynamic forces acting on such model. After that, a physical downsizing model of the airfoil is manufactured and its natural frequencies, damping ratios, and mode shapes are calculated and compared to those obtained from the analytical models. Vibration experiments are also conducted to measure the physical model's structural response in the wind tunnel, and its aerodynamic forces are calculated based on the data recorded by the attached accelerometers.

Keywords: Aircraft wing model, Experimental measurement, Force determination methods, Frequency response function, Multiple-degree-of-freedom system, Vibratory force and moment.

*Corresponding author Yucheng Liu: Department of Mechanical Engineering, Mississippi State University, MS, 39762, USA; Tel/Fax: (001)662-325-1536/662-325-7223; E-mail: yliu@me.msstate.edu.

INTRODUCTION

During flight, aircraft wings always present varying structural responses because subject to varying aerodynamic loadings. The applied aerodynamic loadings and the aircraft wing's structural responses are coupled together to create a complicated vibration effect known as structural coupling dynamics. This effect can reduce the service life of the aircraft significantly. Sometimes, sustained vibration at natural frequencies of airfoils may lead to catastrophic structural failure.

Structural coupling dynamics, first developed in the early 1920's, has become an important concern in design of aircrafts. To date, a number of researchers have dedicated tremendous effort and time to lighten the materials of aircrafts so as to obtain an effective loading capacity. However, as the aircraft speed keeps on increasing, the structural flexibility of the aircrafts receives more design concerns because it may cause serious flutter in the airfoil and other aircraft components.

Considering a typical cross-sectional plane of an airfoil, the gravity center G is located at the 42% ~ 45% of the chord line, and the elasticity center is located at the 38% ~ 40% of the chord line. Therefore, the gravity center is not coincident with the elastic center, which results in a coupling effect between the translational and rotational degree-of-freedom of the wing. This coupling effect and the structure – air coupling effect make it difficult to solve the aerodynamic force of aircraft wings.

The aerodynamic forces, which are extremely difficult to obtain from a flying aircraft, can usually be measured from experimental simulations. As a direct, effective, and easy-to-use approach in the aerodynamic study, experimental methods have been extensively employed to simulate the aircraft's flying condition, so as to measure the aerodynamic forces and the structural responses.

In this chapter, methods are developed for determining the aerodynamic forces acting on the aircraft wings during flight. The methods are initially

developed for a 2DOF linear system, and then extended for a MDOF system developed as a finite element model. Wind tunnel test is then conducted to obtain the physical dynamic parameters. The finite element model and the force determination method are then validated by comparing the analytical results with the experimental results.

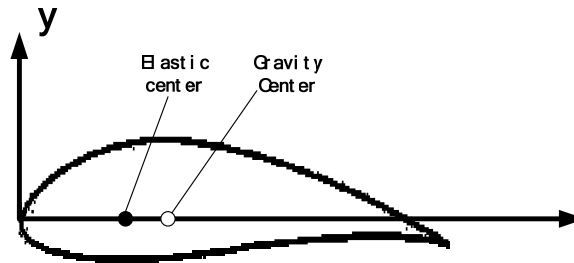


Fig. (1). The schematic diagram for the centers of an airfoil.

LITERATURE REVIEW

Dynamic response of aircraft model during flight has received a lot of interests, and a number of analytical and experimental methods have been developed about the simulating and analyzing the aircraft structures. The literature search focus on two areas: the analytical study of airfoil system and the experimental study of that system.

Analytical Study

Yosibash and Kirby [1] constructed a high order simulation model of fluid-structure for the airfoil under flying conditions. The authors utilized spectral/hp solver for fluid (air) and hp-FEM solver for the airfoil to handle the coupling problem generated by aerodynamic and structure interaction. The two solvers somehow can minimize the modeling errors and the discretization errors. The ongoing verification and validation of fluid-structure interaction are also presented. In their study the airfoil was

CHAPTER 3

Computational and Analytical Investigation of Lateral Impact Behavior of Pressurized Pipelines**Yangqing Dou^{*} and Yucheng Liu***Department of Mechanical Engineering, Mississippi State University, MS 39762, USA*

Abstract: This chapter provides a combined computational and analytical study to investigate the lateral impact behavior of pressurized pipelines and inspect effects of important parameters such as the outside diameter and internal pressure on such behavior. A total of more than 300 numerical simulations are carried out on mild steel pipe models with different internal pressure levels and were struck at the mid-span and at the one quarter span positions. These numerical simulations of the impact tests are performed using 3D dynamic nonlinear finite element analysis (FEA) through LS-DYNA, where both geometrical and material nonlinearities are considered. The computational results for the first time systematically reveal the effects of internal pressure, impact position, and outside diameter on the lateral impact behavior of the pipeline models. Quartic polynomial functions are applied to formulate the maximum crushing force (F_{max}), maximum permanent displacement (W_f), and absorbed energy (E_p) of the pressurized pipelines during the impact problem. The effects of the diameter and pressure on F , W , and E are therefore illustrated through analyzing those functions. Response surfaces are also plotted based on the generated quartic polynomial functions and the quality (accuracy) of

***Corresponding author Yangqing Dou:** Department of Mechanical Engineering, Mississippi State University, MS, 39762, USA; Tel: 337-704-8410; E-mail: yd120@msstate.edu.

Yucheng Liu (Ed.)

All right reserved-© 2016 Bentham Science Publishers

those functions are verified through several techniques. The outcomes of this study have potential benefits on research of safety and reliability of pressurized pipelines in hydraulic system of aerospace and development of advanced pipeline materials.

Keywords: Collapse mechanism, Computer modeling and simulation, Lateral impact, LS-DYNA, Pressurized pipeline.

NOMENCLATURE

$2L$	Distance between two supports of a pipeline
D	Outside diameter of a pipeline
σ_y	Static uniaxial yield stress of pipe
σ_u	Static ultimate tensile stress of pipe
ϵ_r	Static uniaxial rupture strain of pipe
p	Internal pressure
W_f	The maximum permanent transverse displacement
W_l	The local permanent transverse displacement
W_g	The global permanent transverse displacement
F_{max}	Maximum impact force
F_m	Average impact force
v_i	Initial velocity of indenter
v_r	Rebound velocity of indenter
E_p	Absorbed impact energy
E_f	Threshold failure energy

INTRODUCTION

Dynamic responses and failure modes of pipelines subjected to low-velocity lateral impact were studied and described by Jones and other researchers [1-9] through a series of experimental and theoretical analyses. In Jones' work [1-3, 9], pipelines with different sizes were fully clamped at both ends and a rigid indenter struck transversely at the pipe center, quarter span and near to the support at velocities ranging up to 14 m/s.

Important experimental results (deformation mode, maximum permanent transverse displacement, threshold failure energy, *etc.*) were observed and associated with size of the pipelines, initial kinetic energy of the indenter, its impact velocity, and its impact position. In addition, properties of material of the pipelines were also considered and the influences of material strain hardening, strain rate sensitivity, and elasticity on the impact behavior of the pipelines were included in their analytical models. Pressurized pipelines were also tested in Jones' and Ng's work [8, 9] but the influence of internal pressure on the impact behavior of the pipelines has not been explicitly demonstrated. In reality, the internal pressure is a critical factor in the design and assessment of pipelines because in civil applications such as aerospace hydraulic systems, most pipelines convey gases and liquids under high pressures over long distances.

In this study, the dynamic inelastic behavior of clamped thin-walled pipes with internal pressure impacted transversely by a rigid, knife-edge indenter at the pipe center and quarter span is modeled and examined computationally through more than 300 simulations. The obtained numerical results are validated by comparing to several previously published experimental data. Effects of internal pressure on the lateral impact response of the pipelines as well as influences of other impact conditions such as dimensions of the pipelines and impact location are revealed from those simulation results. An explicit FEA solver, LS-DYNA is employed to create the FEA models and run the numerical analyses.

After the computational analysis, numerical methods are employed to establish analytical models to numerically show how the impact parameters (internal pressure and outside diameter) affect the impact response of the pipelines during low-speed lateral impact. This study mainly focuses on finding the effects of internal pressure and outside diameter on the pipeline's impact force, deformation, and energy absorption capacity.

CHAPTER 4

Effect of Bondline Thickness on the Traction-separation Laws of Adhesively Bonded Joint**Gefu Ji¹, Zhenyu Ouyang¹ and Guoqiang Li^{1,2,*}***¹Department of Mechanical & Industrial Engineering, Louisiana State University, Baton Rouge, LA 70803, USA**²Department of Mechanical Engineering, Southern University, Baton Rouge, LA 70813, USA*

Abstract: A number of existing and emerging industrial applications are dependent on layered substrates through adhesive bonding. The interfacial fracture of adhesively bonded structures is a critical issue for their extensive applications to a variety of modern industries. In the recent two decades, cohesive zone models (CZMs) have been receiving intensive attentions for fracture problems in adhesively bonded joints due to its fairly simple and accurate predictive ability. In CZMs the nonlinear interfacial fracture behaviors are described by the traction-separation laws (also referred to as cohesive laws). The cohesive laws represent the local constitutive behavior, instead of the global parameter, such as toughness. While numerous global tests have been conducted to measure the interfacial toughness of adhesive joints, limited local tests have been conducted to determine the interfacial traction-separation laws or interfacial cohesive laws. Among the limited local tests in some recent experimental studies, very few studies have considered the effects of adhesive thickness on the local interfacial traction-separation laws. In the present work, within

*Corresponding author **Guoqiang Li**: Department of Mechanical & Industrial Engineering, Louisiana State University, Baton Rouge, LA 70803, USA; Department of Mechanical Engineering, Southern University, Baton Rouge, LA 70813, USA; Tel/Fax: 001-225-578-5302/001-225-578-5924; E-mail: lguoqi1@lsu.edu

Yucheng Liu (Ed.)

All right reserved-© 2016 Bentham Science Publishers

the framework of nonlinear fracture mechanics, comprehensive experimental studies are conducted to investigate the effect of adhesive layer thickness on the local nonlinear interfacial behaviors. The fracture tests of adhesive joints with various adhesive layer thicknesses were conducted under different fracture modes: pure Mode-I (peel fracture), pure Mode-II (shear fracture), and mixed Mode I/II. The experimentally determined interfacial traction-separation laws provide valuable baseline data for parameter calibrations in numerical models. The current experimental results may also facilitate the understanding of adhesive thickness dependent interface fracture of bonded joints.

Keywords: Adhesive thickness, Bonded joints, Cohesive law, Cohesive strength, Cohesive zone model, Interfacial strength, Plastic zone, Toughness.

INTRODUCTION

Background

Adhesive Bonding Technology

The most primitive form of adhesive bonding technology can be traced back to 200,000 BC when hominins in central Italy glued spear stone flakes to a wood with birch-bark-tar [1]. Today adhesive bonding technology has been used in a wide variety of modern industries, such as automotive, aerospace, marine, construction, and military. Many components and structures, from microchips to large aircrafts, are made of materials arranged in layers through adhesive bonding [2].

The strength of attachment, or adhesion, between an adhesive and its substrate depends on the mechanisms of adhesion and the surface area over which the two materials contact. The mechanisms of adhesion can be categorized as mechanical, chemical, dispersive, electrostatic, or diffusive. Mechanical adhesion occurs when adhesive materials fill the voids or pores of the surfaces and the surfaces are held together by interlocking;

chemical adhesion is developed when the two materials form a compound at the joint; dispersive adhesion is realized through the attraction between two molecules with regions of slight positive and negative charge (*i.e.*, van der Waals forces); electrostatic adhesion happens when some conducting materials pass electrons to form a difference in electrical charge at the joint; finally, diffusive adhesion is realized when the molecules of both materials are mobile and soluble in each other and merge at the joint by diffusion [3].

Three Basic Modes of Fracture

Failure of the adhesive joint imposes a major threat to the reliability of adhesively bonded structures. There are three basic modes of fracture, which are opening (mode I), shear (mode II), and tearing (mode III), as shown in Fig. (1.1). A fracture is considered as Mode I when the tensile stress is normal to the plane of the crack. When the shear stress acts parallel to the plane of the crack and perpendicular to the crack front, the fracture is considered Mode II. Mode III is characterized by a shear stress acting parallel to the plane of the crack and parallel to the crack front. In reality, however, all three modes occur simultaneously. In other words, it is a mixed mode.

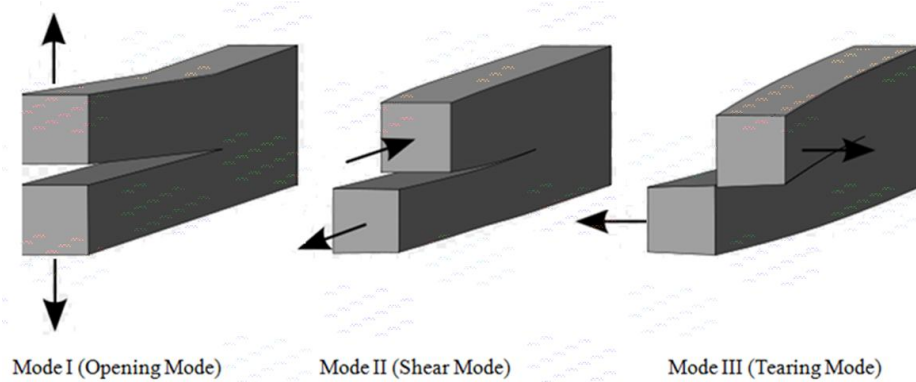


Fig. (1.1). Three basic fracture modes [4].

CHAPTER 5

Optimization of Geometric Parameters and Reversing Design Methodology of Investment**Yangqing Dou^{*}, Yangliu Dou, Kun Bu and Yiwei Dong***Department of Mechanical Engineering, Mississippi State University, MS 39762, USA*

Abstract: With the continual development of the aircraft industry, aircraft engines have provoked people's attention more and more. The turbine blade plays a vital and critical component of aircraft engines. In order to conform to the dimensional tolerances of wax pattern die-profile for turbine blade in investment casting process, this chapter provides an optimization method of geometric parameter for turbine blades based on inverse adjustment. The geometric parameters for optimizing were extracted, and the bending and torsional deformation can be compensation. Therefore the nonlinear deformation compensation during solidification and cooling procedure can be efficiently realized. This method set the theoretical foundation on optimization method of die-cavity for turbine blade. The die-profile optimization system which was developed in this paper proves better effect for the die-cavity design. This chapter also offers a reverse design methodology for investment die casting using ProCAST. In industry, the performance of the engine depends not only on shape, but also on the dimensions of the components. This process is difficult as super-alloy blade material cannot be easily machined. However investment casting is an ideal process for such net - shape components, but it still requires an accurate determination of the casting-die profile. In order to investigate and analyze the methods that affect the shape and dimensions of the turbine blade most, similar

***Corresponding author Yangqing Dou:** Department of Mechanical Engineering, Mississippi State University, MS, 39762, USA; E-mail: yd120@msstate.edu.

Yucheng Liu (Ed.)

All right reserved-© 2016 Bentham Science Publishers

simulations have been conducted by ProCAST. By combining the methods of simplifying grid files and quick sorting, the efficiency of sorting and matching can be largely improved. Furthermore, the mold die cavity anti-deformation system can be easily built by utilizing that reverse design methodology. The optimized die profile for investment casting can be established with ProCAST.

Keywords: Die Cavity, Geometric Parameter, Inverse Deformation, Investment Casting Die, Node Matching, Numerical Simulation, ProCAST, Reversing design methodology, Turbine Blade.

NOMENCLATURE

P	The initial shape before deformation
Q	The shape after deformation
R	The shape after reverse deformation operation
$D(x, y, z)$	Objective function
$P(x, y, z)$	The shape function of turbine blade before investment casting
$Q(x, y, z)$	The shape function of blade after casting process
$W(x, y, z)$	Displacement field function (deformation function) of the each node (x,y,z) in the FEM model
D	The CAD leaf coordinates of i^{th} node
ΔMax	The threshold for maximum error
Q	The simulated surface coordinate of i^{th} node
n	The total number of surface nodes.
M	Shape form error
X	Average form error of width direction
Y	Average form error of thickness direction
Z	Average form error of length direction

INTRODUCTION

Investment casting, or traditionally called lost wax casting process, is to make precise metal product without further machining by pouring the liquid metal into a pre-shaped mold. This process simplifies production by casting a single complex-shaped piece instead of manufacturing a product that requires assembling several pieces together [1]. It is well known that investment casting is used routinely for fabricating single-crystal nickel super-alloy turbine blades. The turbine blades are usually of complex geometries with intricate channels, which allow air to flow within and along the blades during operation [2-3].

A conventional investment casting procedure includes: A. preparing wax patterns by injecting wax into previously designed dies; B. making ceramic shells covering the wax patterns; and C. the alloys are cast into the de-waxed shell molds. It is obvious that the shape of the casting significantly depends on the cavity geometry of the metal die. Due to the shrinkage of the wax and solidification of the alloy material, the size of the component produced by the investment casting process is smaller than that of the die cavity. Although the volume changes in the solidification process are simple in nature, the complex geometry of the turbine blade makes closed-form solutions for the shrinkage almost intractable. Therefore, in order to ensure the dimensional tolerance, the geometrical accuracy and the surface roughness, the design of the die profile for turbine blade needs to consider the compensation of the shrinkages and thermal distortion during solidification [4].

Due to the complex, time-consuming and expensive process of investment casting, traditional methods for designing die profile assumes constant shrinkage rate [5]. However, the complex shape and structure causes uneven heat dissipation during cooling, and thus the non-linear and non-uniform shrinkage distribution. Further considerations have to be given to the shrinkage of wax pattern during preparation; ceramic shell

CHAPTER 6

Vibration Induced Fatigue Analysis of Aerospace Structures**Murat Aykan^{1,*} and Mehmet Çelik²**

¹*Department of Mechanical Engineering, SST Division-ASELSAN Inc., 06172, TURKEY*

²*Department of Mechanical Engineering, MGEO Division-ASELSAN Inc., 06011, TURKEY*

Abstract: This chapter discusses the structural analysis aspects of aerospace structures focusing on vibration induced fatigue. Metal Fatigue of dynamically loaded structures is a very common phenomenon in engineering practice. Several aerospace structures are used in environments where they experience dynamic loading. Furthermore, when the loading is dynamic, the response of the structure is affected by the structural resonances. Thus, the structural response to the loading will amplify at the regions of resonance. As a case study, an antenna (12-59 V/UHF) integration process on helicopter is investigated where the importance of the dynamic response is highlighted. Flight tests and finite element analyses (FEA) are carried out to ensure the safety of the integration process. Furthermore, another important aspect of the structural analysis of aerospace structures is the testing strategy. In this study, the fatigue tests performed by uni-axial tests which is a procedure defined in military standards are compared to multi axial testing. The results are shown for a helicopter Chaff/Flare Dispenser Bracket. The military standards assume that cumulatively uni-axial testing has equal multi axial testing fatigue damage. In this study, the uni-axial

*Corresponding author **Murat Aykan:** Department of Mechanical Engineering, SST Division-ASELSAN Inc., 06172, TURKEY; Tel/Fax: +903125921000; E-mail: m.aykan@hotmail.com.

fatigue tests were compared to multi axial fatigue tests which were performed by FEA simulations. Furthermore, the effects of various loading conditions and geometries were investigated. The study showed that the assumption of multi axial testing can be represented by uni-axial testing does not hold for various cases.

Keywords: Computer modeling and simulation, Multi-axial testing, Uni-axial fatigue testing error, Vibration induced fatigue.

INTRODUCTION

Mechanical structures usually work in a dynamic loading environment and most of the time the loading is repeating itself in time. This repetitive loading doesn't have to be above the yield stress of the structure for failure. Repetitively loading the structure will ultimately cause failure.

This phenomenon is called as Fatigue Failure. Typically, fatigue failure starts at the highest stress zones by forming cracks and then propagates under cyclic loading, where the stress state can be still under the yield point of the material. When a limit is reached for the number of cycles of loading the component fails at a fatigue failure surface. Unfortunately, most of the time fatigue failures cannot be detected until catastrophic accidents occur. In the past, many accidents due to the fatigue failures in metals have occurred. Fig. (1) shows some of them.

Furthermore, according to the survey [3] for helicopter component fatigue failures, these failures are approximately 55% of all premature failures in helicopter components as shown in Table 1.

This chapter will consist of two case studies which will focus on different analysis and testing aspects of aerospace structures. The first section will investigate an antenna integration process including flight tests and stress analysis where the structure will not require fatigue analysis [4]. The antenna is part of the MXF-484 V/UHF transmitter, which is used to safely communicate without any enemy interference. Fig. (2) shows the integration area on the helicopter.

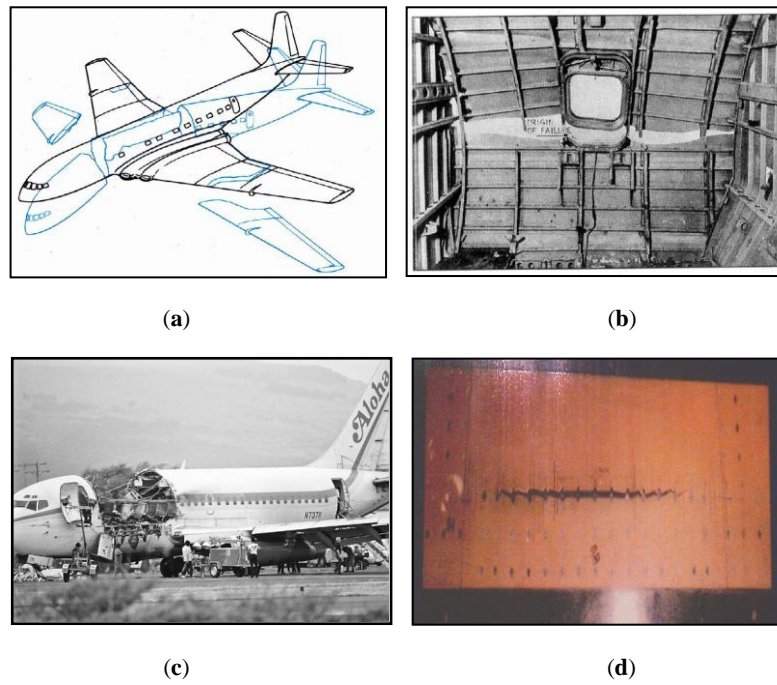


Fig. (1). (a) Comet fuselage failure (b) Stress concentrations at window corners [1] (c) Aloha Airlines Boeing 737 fuselage failure due to multiple cracks at rivet holes (d) Crack growth on fuselage [2].

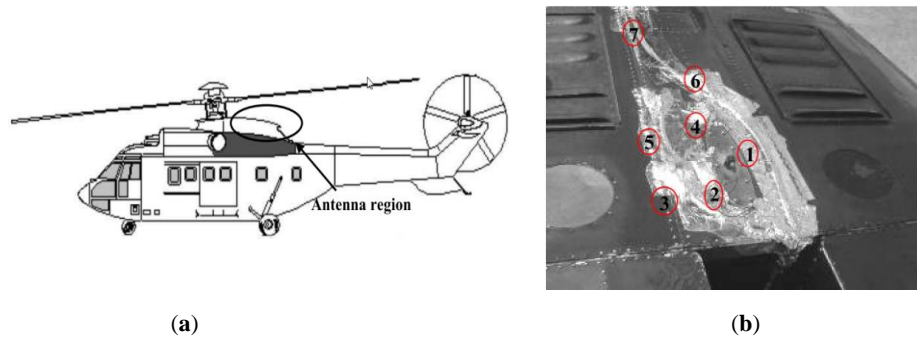


Fig. (2). (a) Antenna location on helicopter, (b) Measurement locations when antenna is not installed.

Fatigue Life Optimization of Laser Peened Aircraft Components

Anoop Vasu* and Ramana V. Grandhi

Department of Mechanical and Materials Engineering, Wright State University, Dayton, OH 45435, USA

Abstract: Surface treatments, such as laser peening, can increase the life of the component by generating compressive residual stresses on the surface. Laser peening of an already peened component, termed as re-peening, can further increase the fatigue life of the component. Re-peening has several applications in the aerospace industry. The huge population of ageing aircraft components is one such application, which can benefit significantly from the re-peening process. However, this process is not optimized for maximum fatigue life due to the presence of many design variables and the complex nature of the problem which requires a large number of experimental testing to reach conclusions. Therefore, a computationally efficient optimization strategy needs to be developed to conduct large-scale laser peening simulations for problems related to fatigue life, such as aircraft lug failure, a problem that requires consideration of component curvature and residual stress relaxation effects. Deciding the time to peen an already peened component (re-peening time) is another variable which makes the problem further complicated. The ultimate goal of this research is to construct the framework to predict the optimum parameters for maximum fatigue life on structural components. A two-step optimization strategy is adopted for the fatigue life optimization of an aircraft lug component. The strategy

*Corresponding author Anoop Vasu: Department of Mechanical and Materials Engineering, Wright State University, Dayton, OH 45435, USA; Tel/Fax: 937-775-5040; E-mail: anoop1984@gmail.com.

Yucheng Liu (Ed.)

All right reserved-© 2016 Bentham Science Publishers

employs laser peening process parameters, residual stress relaxation, and re-peening schedule as design variables.

Keywords: Fatigue life optimization, Laser peening, Re-peening, Residual stress relaxation.

NOMENCLATURE

R	Relaxation coefficient
N	Number of load cycles
σ_a	Alternating stress
σ_m	initial mean stress
σ_I	Mean stress after one cycle
σ_y	Material yield strength
σ_u	Ultimate strength
σ_r	Residual stress
σ_{Nf}	Fatigue strength
N_f	Number of cycles to failure
D	Cumulative damage
P	Peak pressure of laser pulse
O	Percentage overlaps of sequential laser spots
t	Mid-span duration of laser pulse
σ_{CRS}	Compressive residual stress
σ_{TRS}	Tensile residual stress

INTRODUCTION

The potential reason for fatigue failure on structural components is the generation of tensile stresses on component surface. These surface regions become the hot spot to initiate cracks. Generation of compressive residual stresses can inhibit or delay the crack initiation and growth. Surface enhancement techniques can generate compressive residual stresses and hence play an important role in improving the life of the peened

components [1]. Shot peening is the most commonly used mechanical surface treatment method. Other widely applied methods in the industry are low plasticity burnishing, water jet peening, laser peening, roller burnishing, ultrasonic peening, peen forming, cavity peening, *etc.* Laser peening generates deeper compressive stresses compared to other surface treatments like shot peening, making it appealing to the industry. Fig. (1) shows the fatigue effect of the material Al 7075-T7351 treated by laser peening with comparison to unpeened and shot peened materials (bending tests, stress ratio=0.1) [2]. This shows that laser peened material has an improved fatigue life.

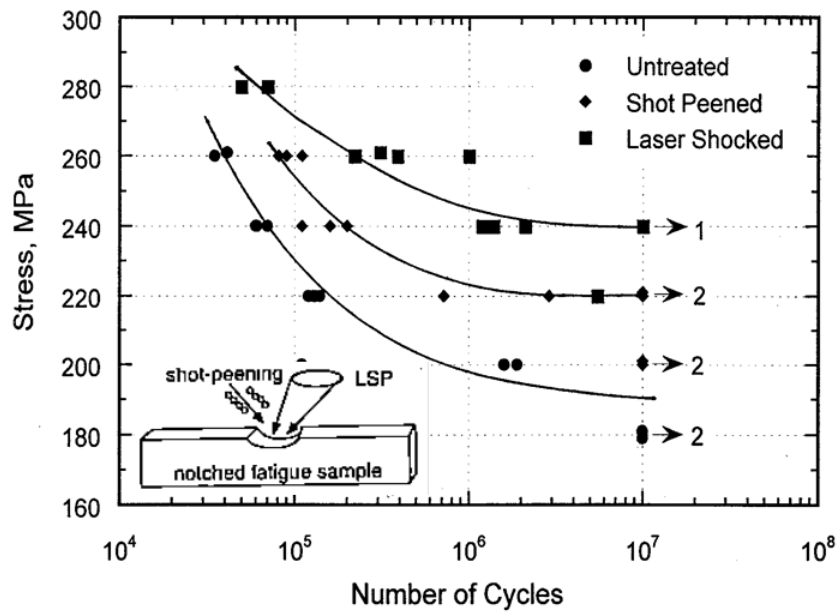


Fig. (1). Fatigue life comparison for Al 7075-T7351.

A pictorial representation of a typical laser peening method is shown in Fig. (2). The target material is typically coated with an ablative overlay and confined by a transparent overlay. When the laser pulse impacts the material, the absorbent material vaporizes and creates plasma. This

Prediction of Residual Stress Relaxation in Ti-6Al-4V subjected to Laser Peening

Anoop Vasu* and Ramana V. Grandhi

Department of Mechanical and Materials Engineering, Wright State University, Dayton, OH 45435, USA

Abstract: Laser peening is an advanced surface enhanced method which induces compressive residual stress on the critical regions of components prone to fatigue failure. However, the residual stresses relax under the fatigue loading conditions. Constitutive models have to be robust enough to predict the residual stress relaxation mechanism. Although tensile cold working increases the tensile yield strength, the compressive yield strength is reduced. As a result of this, a lower compressive load can relax the initial compressive residual stress. This phenomenon, termed as Bauschinger Effect, can be represented by an analytical stress-strain model to predict the relaxation effects based on the cold working of the material. Three dimensional finite element (FE) models are created to represent residual stress relaxation in a low cycle fatigue regime for Ti-6Al-4V material. The creation of the numerical model for simulating stress relaxation model involves two phases. The first phase is modeling the stress gradient effect which relates to the effect of cold working. This process utilizes a laser peening simulation model. The second phase is modeling the stress-strain response of the material by creating a mixed hardening model.

Keywords: Finite element analysis, Laser peening, Low cycle fatigue,

*Corresponding author Anoop Vasu: Department of Mechanical and Materials Engineering, Wright State University, Dayton, OH 45435, USA; Tel/Fax: 937-775-5040; E-mail: anoop1984@gmail.com.

Yucheng Liu (Ed.)

All right reserved-© 2016 Bentham Science Publishers

Mixed hardening, Residual stress relaxation, Surface enhancement technique.

NOMENCLATURE

<i>HEL</i>	Hugoniot elastic limit
σ_y^{dyn}	Dynamic yield stress
ν	Poissons ratio
σ_{vm}	Equivalent von mises stress
<i>A</i>	Yield stress
<i>B</i>	Strain hardening coefficient
<i>n</i>	Strain hardening exponent
<i>C</i>	Strain rate sensitivity constant
ϵ_p	Equivalent plastic strain
$\dot{\epsilon}^*$	Dimensionless strain rate
$\dot{\epsilon}$	Strain rate from high strain rate experiments
$\dot{\epsilon}_0$	Reference strain rate
d_p	Heat penetration depth
<i>D</i>	Heat diffusion coefficient
τ	Laser pulse width
<i>C_I</i>	Kinematic hardening modulus
σ_{ij}	stress tensor
α_{ij}	Backstress tensor
σ_0	Equivalent stress defining size of yield surface
$\dot{\epsilon}^p$	Equivalent plastic strain rate
γ	Material constant from cyclic test data
$\dot{\epsilon}_{ij}^p$	Rate of plastic flow
<i>R</i>	Stress ratio

INTRODUCTION

How to prevent failure in materials has been a great research interest all over the world for centuries. It has been found out that cyclic loading is a major cause of failure in many situations. There can be other contributing factors, such as manufacturing defects and the presence of unfavorable residual stresses. But residual stresses can also play a positive role and can enhance the life of the component, if applied properly. There exist methods named Surface enhancement techniques (SET), which can induce favorable residual stresses (mechanical SET) on surface regions of peened components to improve the fatigue life of the component [1]. Fig. (1) depicts a pictorial representation of the impact of SET on fatigue life.

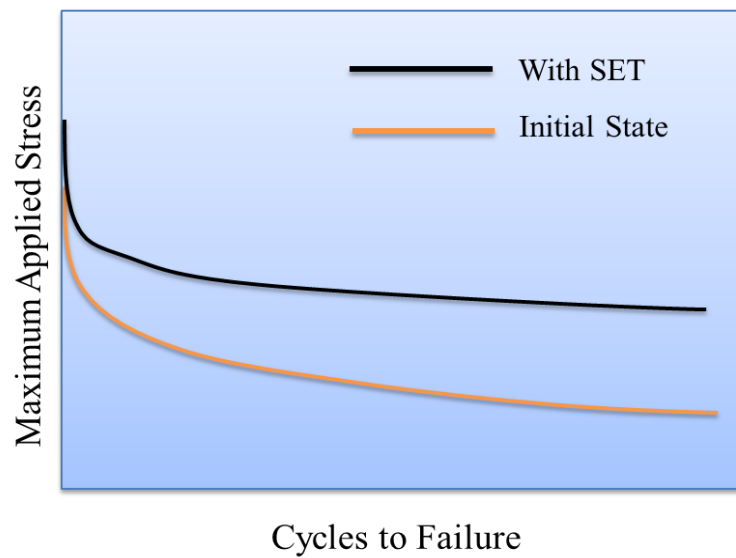


Fig. (1). Extended fatigue life in peened components.

Fig. (2) shows the mechanism behind the mechanical surface enhancement methods. When the material is peened under loading, the surface region in contact would be plastically deformed. The surrounding

Non-Destructive Evaluation (NDE) of Welded Structures for Aerospace Applications

Mohammad W. Dewan, Daniel J. Huggett, and Muhammad A. Wahab*

Department of Mechanical and Industrial Engineering, Louisiana State University, Baton Rouge, LA 70803, USA

Abstract: The aerospace industry has utilized high strength aluminum alloys to propel the production and manufacturing of advanced aerospace technology; however, welding of Aluminum and its constituent alloys introduce challenges which affect the structural integrity of the welded area if conducted indecorously. For this reason, Non-destructive Evaluation (NDE) of welded areas is conducted to ascertain defective regions to ensure structural integrity of the aerospace structure. NDE techniques are noninvasive and can determine whether the object contains irregularities, discontinuities, or flaws. Inspecting weld areas allows for cost reduction by detecting discontinuities in the early stages of manufacturing; consequently, reducing the time and money to rework the error and allows for the validation of sound welds. A variety of NDE techniques are available depending on the applications, each with its own advantages and disadvantages. Among the number of NDE techniques, radiography and ultrasonics are the most widely utilized for inspection of weld defects. In this study, a detailed analysis was thereby conducted to ascertain the critical phased array ultrasonic testing (PAUT) parameters for the detection of weld defects, more specifically with Friction-Stir-Welding (FSW). Consequently a comparison to X-ray radiography is also included. It was observed

*Corresponding author **Muhammad A. Wahab**: Department of Mechanical and Industrial Engineering, Louisiana State University, Baton Rouge, LA 70803, USA; Tel/Fax: (1) 225 578 5823/(1) 225 578-5924; E-mail: wahab@me.lsu.edu.

Yucheng Liu (Ed.)

All right reserved-© 2016 Bentham Science Publishers

that both techniques produced similar detection results for defects in the range of 1.0mm; however, it was found that PAUT was the only technique able to discover defects in the range of 0.15 mm.

Keywords: Non-destructive evaluations, Phased array ultrasonic testing, Radiographic testing, Welding, Welding defects.

INTRODUCTION

Welding is an essential manufacturing process performed in almost every major industry; however, in many welding techniques flaws or defects are quite common in the welded joints. These defects can be found in the form of surface or sub-surface cracks, undercut, porosity, or inclusions [1-3]; and consequently, failure can occur from these flaws [4]. An important decision must be made regarding severity of these weld defects and their effect on the strength; therefore, weld quality and integrity are critical to safety in an extremely wide range of products and structures, especially in the aerospace industry. To ensure sound welds have been forged, Non-destructive Evaluation (NDE) techniques can be employed to determine if defects have formed [5]. Different NDE methods can identify cracking, porosity, incomplete penetration, misalignment, inclusions, and lack of fusion which all can compromise weld strength and eventually structural integrity under dynamic loading conditions.

NDE techniques are utilized in a multitude of scenarios including: Determination whether an object is acceptable after each fabrication step (in-process inspection), determining whether an object is acceptable for final use (Final inspection), and lastly, determining whether an existing object already in use is acceptable for continued uses (in-service inspection). To summarize, NDE is applied to find welding defects as well as quality assurance/quality control (QA/QC) of welded structures [6]. The most common NDE techniques to conduct various inspections are:

Ultrasonic Testing (UT), Radiographic Testing (RT), Liquid Penetrant Testing (LPT), Magnetic Particle Testing (MT), Eddy Current Testing (ET), and Acoustic Emission (AE) testing. Each NDE technique discussed previously has distinct advantages and disadvantages; consequently, depending on the application one technique may be better suited than another. Table 1 briefly illustrates NDE techniques and their principle of operation, applications, limitations, advantages, and welding defects that can be determined. It is noted that NDE techniques rely heavily on human skills and knowledge to correctly assess and interpret results. Proper and adequate training, developing confidence, and appropriate certifications are required to perform non-destructive testing (NDT) [7, 8]. Therefore, flaws or defects are often dictated by a code or requirement which indicates acceptable tolerances, *i.e.* The American Society of Mechanical Engineers Pressure Vessel Code [9] and American Welding Society Structural Welding Code [10-12].

Among the number of NDE techniques, ultrasonics and radiography are the most widely used for checking for weld defects. In recent years, the conventional ultrasonic testing technique has been replaced with more reliable and technologically advanced techniques of Phased Array Ultrasonic Testing (PAUT) and Time of Flight Diffraction (TOFD). Alternatively, radiography is utilized providing a range of techniques from traditional X-ray generators and film to newer technologies such as Computed Radiography (CR), Direct Radiography (DR), and 3D Computed Tomography (CT). These new technologies allow for remote visual inspection and enhancement of data visualization.

Table 1. Common NDT techniques and their applications [9].

Method	Principle of Operation	Application	Limitations	Advantages	Welding Defects
Penetrant Testing	Liquid dye penetrant into cracks and make visible	Surface defects	Will not find subsurface or	Easy and can be used in complex	Burn Through, Surface Porosity, Surface crack,

CHAPTER 10

Development of a Remotely Piloted Helicopter for Civil Applications

N. Goudarzi^{1,*}, R. M. Ziazi², F. Kermanshahi³, S. Sadati⁴, M. S. Sajedi⁵,
and M. Mohagheghi⁶

¹ *Department of Engineering Technology and Construction Management,
University of North Carolina at Charlotte, NC, USA*

² *School of Mechanical, Industrial, and Manufacturing Engineering,
Oregon State University, OR, USA*

³ *Ecole Polytechnique de Montreal, Quebec, Canada*

⁴ *Sustainable Environment and Energy Systems Department, Middle East
Technical University, Northern Cyprus Campus, Turkey*

⁵ *Aerospace Engineering Department, Amirkabir University of Technology,
Tehran, Iran*

⁶ *Aerospace Engineering Department, University of Tehran, Tehran, Iran*

Abstract: An applicable procedure for design, optimization, and manufacturing of a remotely piloted helicopter (RPH) is studied analytically and experimentally. The procedure is presented in four main phases of conceptual design, detailed design, manufacturing and assembly, and test and reliability analysis. Using this procedure, an RPH case study, called Parvan, for an arbitrary traffic monitoring mission is

*Corresponding author Navid Goudarzi: Department of Engineering Technology and Construction University of North Carolina at Charlotte, NC, USA; Tel/Fax: 704-687-5056; E-mail: navid.goudarzi@uncc.edu.

designed and manufactured. Different subsystems of an RPH such as rotor assembly, engine and fuel systems, power transmission system, and control system for the proposed design are studied at each phase accordingly. Finally, 3-D multiplatform software of CATIA is used to simulate the RPH and making the full-scaled prototype. The successful performance of Parvan at hover, climb, and forward flight modes showed the effectiveness of the proposed procedure in developing an RPH.

Keywords: Aerodynamic derivatives, Design experiments method, Dynamic modeling, 3-D simulation, Manufacturing, Optimum design, Reliability, Remotely piloted helicopter, Stability and control, Unmanned aerial vehicle.

NOMENCLATURE

Symbol	Description
Acronyms	
FMEA	Failure Modes and Effect Analysis
FMECA	Failure Modes, Effects, and Criticality Analysis
MTBF	Mean Time between Failures - <i>s</i>
MTTF	Mean Time to Failure - <i>s</i>
PDF	Probability Density Function
RPH	Remotely Piloted Helicopter
UAV	Unmanned Aerial Vehicle
Greek Symbols	
$\beta_{c,CR}$	Control rotor longitudinal flapping - <i>rad</i>
$\beta_{s,CR}$	Control rotor lateral flapping - <i>rad</i>
$\lambda_s(t)$	Failure rate - <i>s</i>
Ω	Rotational speed - <i>rad/s</i>
ρ	Air density - <i>kg/m³</i>
σ	Solidity factor
θ_{OM}	Main rotor blade pitching angle - <i>rad</i>

Θ_{OT} Tail rotor blade pitching angle - *rad*

Roman Symbols

\dot{V}	Acceleration - m/s^2
A	Rotor swept area – m^2
A_l	Lateral cyclic pitch - <i>rad</i>
B_l	Longitudinal cyclic pitch - <i>rad</i>
C	Criticality number
C_D	Drag coefficient
C_l	Lift coefficient
C_p	Power coefficient
C_T	Thrust coefficient
E	Hinge offset - <i>m</i>
F	Force exerted on the body - <i>N</i>
I_{bf}	Moment of inertia for body frame – $kg.m^2$
M	Pitching moment - <i>N.m</i>
m	Mass - <i>kg</i>
P	Power - <i>W</i>
p	Pitching rate - <i>rad/s</i>
P_i	Induced power - <i>W</i>
P_o	Profile power - <i>W</i>
Q	Torque - <i>N.m</i>
q	Rolling rate - <i>rad/s</i>
R	Rotor radius - <i>m</i>
R_y	Rotor moment - <i>N.m</i>
ROC	Rate of climb - <i>m/min</i>
w_{bf}	The matrix of rotational rates of body frame
X	Force acting in x direction – <i>N</i>
Y	Force acting in y direction – <i>N</i>
Z	Force acting in z direction - <i>N</i>

CHAPTER 11

Materials Selection in Design of Structures of Subsonic and Supersonic Aircrafts**Zainul Huda****Department of Mechanical Engineering, King Abdulaziz University, Jeddah 21589, Saudi Arabia*

Abstract: This chapter reviews the advances in the materials for applications in structures of both subsonics well as supersonic aircrafts. An account of the operating and ambient environmental conditions during flight is first given and the resulting material requirements have been discussed. Design relationships have been established taking into consideration the loading conditions and the strength requirements. In particular, the aircraft skin temperatures at various mach numbers have been taken into account for selecting appropriate structural materials for both subsonic and supersonic aircrafts; and consequently various aerospace aluminum alloys, titanium alloys, superalloys, and composites have been suggested. Finally, a new materials-selection chart is presented which would help aerospace designers to select appropriate materials for structural application in subsonic and supersonic aircrafts.

Keywords: Aluminum alloys, Composites, Materials selection, Subsonic aircraft, Supersonic aircrafts, Titanium alloys.

*Corresponding author **Zainul Huda:** Department of Mechanical Engineering, King Abdulaziz University, Jeddah 21589, Saudi Arabia; Tel/Fax: +966537701246; E-mail: drzainulhuda@hotmail.com.

NOMENCLATURE

M	Mach number
CT	Civil transport
SST	Supersonic transport
CFRP	Carbon fiber reinforced polymer
SCC	Stress corrosion cracking
$W_{(a)}$	Weight of a structural member using material (a)
$W_{(b)}$	Weight of a structural member using material (b)
$\rho_{(a)}$	Density of material (a),
$\rho_{(b)}$	Density of material (b),
$\sigma_{y(a)}$	Yield strength of material (a)
$\sigma_{y(b)}$	Yield strength of material (b)
$\tau_{(a)}$	Torsional shear stresses acting on materials (a)
$\tau_{(b)}$	Torsional shear stresses acting on materials (b)
E	Young's modulus
K	Stress intensity factor
K_{IC}	Plane strain fracture toughness
σ	Stress applied normal to a crack
RMAF	Royal Malaysian Air Force
Al-Cu	Aluminum-copper alloy
P/M	Powder metallurgy
Ti-Al-V	Titanium-aluminum-vanadium alloy
UTS	Ultimate tensile strength
BMI	Bismaleimides
CE	Cyanate esters
FGM	Functionally graded materials

INTRODUCTION

The design of an aircraft and its materials have to be determined based on classical engineering principles and practices because even a tiny mistake in the design of any critical aircraft components such as fuselage, skeleton,

and wing may lead to fatality. A subsonic aircraft is an aircraft with a maximum speed less than the Mach 1 (speed of sound) *i.e.* less than 750 mi/h (1207 km/h). On the other hand, supersonic aircrafts have the capacity of flying at speeds greater than Mach one, $1 < M < 4$. Currently, supersonic aircrafts fly at speeds less than 2000 mi/h (3219 km/h). The important factors in selecting aircraft materials include specific strength (strength-to-weight ratio), tensile mechanical properties, fatigue strength, low-speed impact strength, fracture toughness, notch sensitivity, manufacturability, resistances to crack propagation, stress corrosion, and exfoliation corrosion [1-3]. Extra material criterion, exclusively related to the design of supersonic aircraft, is the resistance to creep. This is because the long-term operation at Mach 3.5 may lead to heat buildup within the structure of the aircraft to a temperature around 300 °C [4, 5].

Having established the material requirements for application in structures of subsonic and supersonic aircrafts in the preceding paragraph, it is appropriate to discuss the performance the aerospace structural materials; the latter include aluminum alloys, titanium alloys, and composites. This paragraph deals with aerospace alloys for subsonic aircrafts. A high-priority material research focus in today's civil-transport (CT) aerospace industry is the development of aluminum alloys with higher specific strength (strength/weight ratio) for subsonic aircrafts; this research focus is obviously owing to lower cost of aluminum as compared to titanium and composites. The 2024 and 7075 aluminum alloys have remained in long use in CT subsonic aircrafts. For instance, age-hardenable 2024-T3 aluminum alloy is used in the subsonic structure: an aircraft for military transport application. The 7075-T6 Al alloy sheets and plate products have applications in subsonic aircraft structures owing to their notable combination of high strength with moderate toughness and corrosion resistance [6, 7]. In addition to Al alloys, titanium aerospace alloys are known for their high specific strength, moderately high-temperature stability, and resistance to corrosion. The exceptionally attractive

Potential Aerospace Applications of Carbon Nanotubes

Omid Gohardani*

Springs of Dreams Corporation, 340 East 1st Street, No. 8, Tustin, California 92781, United States of America, USA

Abstract: Advanced materials with optimized properties are essential in addressing the stringent requirements imposed by future aerospace vehicles. The discovery of carbon nanotubes and their desirable properties, as recognized in diverse scientific disciplines, have therefore identified these materials as expedient candidates for usage in aerospace applications. Given the limited number of overarching review articles encapsulating the usefulness of carbon nanotubes in aerospace sciences, this chapter explores the prospective applications of these materials in aerospace applications with their possible implementation on future aircraft, unmanned aerial vehicles and rotorcraft. The prospects of carbon nanotube usage intended for fuselage/satellite weight reduction, aircraft icing mitigation, lightning protection for aircraft, and future space launch are further explored. Conclusively, present challenges associated with successful implementations of these materials and existing obstacles preventing their safe integration in the aerospace industry are revisited, outlined and discussed.

Keywords: Aerospace nanotechnology, Aircraft icing mitigation, Carbon nanotubes, Future aerospace materials, Hydrophobicity, Space elevator.

*Corresponding author Omid Gohardani: Springs of Dreams Corporation, 340 East 1st Street, No. 8, Tustin, California 92781, U.S.A; E-mail: omid.gohardani@springsofdreams.org.

Yucheng Liu (Ed.)

All right reserved-© 2016 Bentham Science Publishers

NOMENCLATURE

ρ	Density
ζ	Electrical resistivity
σ_{\max}	Tensile strength
d_t	Nanotube diameter
k	Thermal conductivity
m, n	Integers
AR	Aspect ratio
C_h	Chiral vector
E	Young's modulus

INTRODUCTION

Carbon nanotubes (CNTs) have since their relatively recent discovery, been employed in a multitude of different scientific applications such as sensing [1], mechanical systems [2], energy storage [3, 4], biological applications [5, 6], and field emission [7, 8]. The expanding usage of composite materials on current commercial and military aircraft has in this respect highlighted these materials as viable candidates that can sustain different operational requirements in aeronautics and astronautics.

This chapter provides an introduction to CNTs, by means of a brief historical overview of CNT usage in aerospace applications, viewed through the lens of the aerospace industry and further investigates their prospective usage areas in aeronautics and astronautics. In this context, particular attention is devoted to potential benefits of CNTs intended for unmanned aerial vehicles (UAVs) and their proposed usage, and other aspects pertaining to future space launch platforms. The final discussion of this chapter features a review of obstacles that have prevented a more frequent utilization of CNTs in the aerospace industry and establishes

essential factors for such implementation.

In essence, CNTs are commonly described in the literature in two distinct forms namely, single-walled carbon nanotubes (SWCNTs) and multi-walled carbon nanotubes (MWCNTs) [9]. SWCNTs consist of single tubular sheets of graphite while the latter comprise a family of concentric graphite tubes [10]. For SWCNTs, the roll direction of the graphite sheet and the tube structure denoted by the integers n and m , determines the conductivity. The chiral vector is defined as $\mathbf{C}_h \equiv (n, m)$ [11], where the values of m and n determine the structure of the nanotube as an armchair ($n = m$), zigzag ($m = 0$) and chiral (other n and m values than the previous two structures). An overview of the properties of SWCNTs and MWCNTs, in comparison to traditional aerospace materials, is shown in Table 1.

Table 1. Comparison of CNTs to conventional materials. The symbol (*) distinguishes normalized values, while (†) and (‡) denote theoretical and measured values, respectively. (Sources: [12, 13]).

Material	Specific Gravity [g·cm ⁻³]	Yield Strength [GPa]	Elastic Modulus [GPa]	Thermal Conductivity [W·m ⁻¹ ·K ⁻¹]	Electrical Resistivity [μΩ·cm]	Strength-to-Mass Ratio*
SWCNTs [†]	1.4	65	1,000	~ 6,000	30–100	225
SWCNTs [‡]	1.4	1.8	80	150	150	7
Conventional Carbon fiber, M55J	2.2	4	550	70	800	9
IM7 Carbon composites	1.6	2.1	152	30	2,000	7
Titanium	4.5	0.9	103	12	127	1
Aluminum	2.7	0.5	69	180	4.3	1

A comparison between density (ρ), nanotube diameter (d_t), aspect ratio

CHAPTER 13

Combination of Carbon Fiber Sheet Molding Compound and Pre-Impregnated, Tailored Carbon Fiber Reinforcements

Marc Fette^{1,3,*}, Nicole Stöß², Jens Wulfsberg¹, Axel Herrmann³,
Gerhard Ziegmann⁴ and Georg Lonsdorfer³

¹*Institute of Production Engineering, Helmut Schmidt University, 22043 Hamburg, Germany*

²*Polynt Composites Germany GmbH, Kieselstraße 2, 56357 Miehlen, Germany*

³*Composite Technology Center GmbH (An Airbus Company), Airbusstraße 1, 21648 Stade, Germany*

⁴*Institute of Polymer Materials and Plastics Engineering, TU Clausthal, Agricolastrasse 6, 38678 Clausthal, Germany*

Abstract: The current use of fuel efficient and environmentally friendly aircraft is only possible by the development of innovative lightweight constructions and the use of lightweight materials, such as carbon fiber reinforced plastics. With the rising demand on fiber reinforced components in the aerospace industry new production processes have been built up. However, current production technologies for composites cause higher costs and obtain longer process cycle times in comparison to the manufacturing processes of metals. Moreover raw materials, such as carbon fibers and resin, and semi-finished products are very expensive. In contrast to this and compared with other manufacturing technologies for fiber reinforced plastics

*Corresponding author **Marc Fette:** Institute of Production Engineering, Helmut Schmidt University, Hamburg, Germany; E-mail: marc.fette@hsu-hh.de.

Yucheng Liu (Ed.)

All right reserved-© 2016 Bentham Science Publishers

Sheet Molding Compound compression processes are characterized by cost efficiency, high productivity, the option of full automation and the possibility for the realization of complex shapes and integrated functions. However there are also some disadvantages like a low level of stiffness and strength in comparison to continuous fiber reinforced plastics. The reasons for these facts are the short fibre length, a lower fibre-volume fraction and an isotropic fibre distribution. Consequently, the combination of sheet moulding compound and pre-impregnated, tailored carbon fibre reinforcements in an one-shot compression moulding and curing process merges the advantages of both groups of composite materials. Therefore the creation of load-bearing, complex, functional and autoclave-quality parts without an autoclave can be realised. In this chapter, this innovative technology and its potentials are presented. This paper will also deal with the resulting material characteristics.

Keywords: Aircraft, CFRP, Hybrid, Light weight, SMC.

NOMENCLATURE

ATH	Aluminum hydroxide or alumina trihydrate
CFRP	Carbon fiber reinforced plastic
FRP	Fiber reinforced plastic
SEM	Scanning electron microscope
SMC	Sheet Molding Compound
UP	Unsaturated polyester resin

INTRODUCTION

In the recent decades, the demand for efficient and fuel-saving aircraft for the commercial air traffic has led to the development of innovative lightweight solutions and to an increasing use of modern lightweight

materials, such as carbon fiber reinforced plastics (CFRP). In this context the aerospace industry developed new manufacturing processes and enhanced existing technologies to produce such high-performance materials. However, the today's production of aerospace components made of FRP materials is time-consuming and costly in comparison to the production of metallic constructions. Reasons for this are relatively high costs of raw materials and semi-finished products, long processing times and a partially low degree of automation. As a result there exist lots of aspirations for the development of more efficient technologies, the optimization of existing processes or the smart combination of different technologies.

One promising technology is the combination of carbon fiber Sheet Molding Compound (SMC) and pre-impregnated, continuous carbon fiber reinforcements in a one-step compression and curing process. In this context the SMC technology provides the implementation of light, geometrically complex and highly functional composite components considering short cycle times, an optimum usage of material, the possibility of complete automation and high cost efficiency. The locally integrated continuous carbon fiber reinforcements obtain tailored mechanical properties depending on the load characteristics of the respective component and with regard to the required high lightweight potential. In addition, this hybrid composite technology promises the possibility of using of recycled carbon fibers as long fiber reinforcements in the SMC mass and the direct integration of metallic components. This material and process combination can realize light weight, complex and functional composite components for aerospace applications in a highly efficient way.

The main objectives of this article are researches and analysis of the potentials of this technology in reference to aerospace applications with the requirements for secondary structures of commercial aircraft.

CHAPTER 14

Design Optimization of Variable Stiffness Composite Structures for Aerospace Applications

Mohammad Rouhi*, Hossein Ghayoor, Suong V. Hoa and Mehdi Hojjati

Concordia Center for Composites, Department of Mechanical and Industrial Engineering, Concordia University, Montreal, Quebec, H3G 1M, Canada

Abstract: Automated fiber placement (AFP) machines can steer the fibers/tows to make the so-called variable stiffness (VS) composites. They allow the designers to fully exploit the directional properties of composite materials to tailor the internal load distribution and improve the structural performance. VS composites have been shown to be very promising in the design optimization of composite panels and shells for buckling and post-buckling performance and consequently for further reducing the mass of future aerospace structures. In this chapter, the buckling performance improvement of VS composite cylinders with circular and elliptical cross sections is investigated. A metamodeling based design optimization (MBDO) method is presented to maximize the buckling performance of VS composite cylinders compared with their constant

*Corresponding author **Mohammad Rouhi:** Concordia Center for Composites, Department of Mechanical and Industrial Engineering, Concordia University, Montreal, Quebec, H3G 1M8 Canada; Tel/Fax: 514 - 848 4596; E-mail: m.rouhi@gmail.com

Yucheng Liu (Ed.)

All right reserved-© 2016 Bentham Science Publishers

stiffness (CS) designs. The structural improvement mechanism via stiffness tailoring in a VS composite cylinder is also presented and discussed. The effects of different parameters including the cylinders' aspect ratio and size as well as the percentage of the steered plies in the laminate are also investigated.

Keywords: Automated fiber placement, Buckling, Composite cylinder, Fiber steering, Optimization, Variable stiffness.

INTRODUCTION

Lightweight and high performance are essential requirements for aerospace structures. In case of using metallic materials, designers put all their effort to reduce the weight and optimize the structural performance by tailoring the topology and shape of the structure *i.e.* thickness, size, and overall profile/shape. Over the past few decades, the application of fiber-reinforced polymer composite (FRPC) materials in aerospace structures has been increased dramatically. This growth has primarily been fueled by the high stiffness- and strength-to-weight ratios of FRPC materials as well as tailorability of the stiffness and strength properties and substantial reduction in part count offered by such material systems. Unlike metallic structures, composite structures can be manufactured in very complex geometric shapes. Consequently, FRPC materials can help enhance both product performance and manufacturing.

FRPC materials have traditionally been designed and manufactured as multi-ply laminates consisting of several unidirectional layers. The layers are either stacked in dry form with the polymer resin injected into the mold or the layers are pre-impregnated with the resin material prior to manufacturing. In either case, for product design and manufacturing simplicity, the fiber orientation angle in each layer is typically held fixed and usually limited to 0° , 90° , and $\pm 45^\circ$. By limiting each layer to a single orientation angle over the entire structural component, the designer is

unable to fully exploit the directional material properties offered by composite layers. On the other hand, without sophisticated manufacturing equipment, it would be nearly impossible to accommodate spatial variation of orientation angles in the individual plies. With the advent of Automated Fiber Placement (AFP) machines, it has become possible to steer the fibers to manufacture composite parts with continuously varying fiber orientation angles. The resulting so-called variable stiffness (VS) laminate has spatial stiffness properties that allow the full potential of composite materials to be harnessed by extending the design space to create structural components with significantly higher performance and/or lower weight [1-5]. However, there are several design and manufacturing challenges that need to be addressed to reach the full potential of VS composite structures made by fiber steering.

Early research works on AFP technology were reported in the literature in the late 1980's [6]. Followed by building composite stiffened panels by AFP machines [7, 8] in the early 1990's, AFP technology was used in production of numerous aircraft parts such as the F/A-18E/F horizontal stabilizer skins, the Bell/Boeing V-22 Osprey aft fuselage [9, 10], the V-22 grip [11-13], the Boeing JSF inlet duct and the C17 landing gear pod fairings and engine nacelle doors [9,14], and the fuselage sections of Raytheon Premier I and Hawker Horizon business jets [15]. The recent application of AFP technology includes the large scale production of the fuselage sections of the Boeing 787 Dreamliner, Airbus A380 and A350 XWB [16, 17]. The overall saved labor costs and reduced scrap materials, combined with the ability to produce laminated composite components of exceptional quality with higher accuracy and repeatability, have been shown to cover the substantial investment required by AFP technology.

VS composites have been extensively studied for several loading scenarios and different structures such as plates [2, 18-21] and cylindrical shells [4, 5, 22-24] to examine the effect of fiber steering in improving structural performance and reducing weight. Since in aerospace structures

CHAPTER 15

Manufacturing Challenges Associated with the Use of Metal Matrix Composites in Aerospace Structures

Tracie Prater*

NASA Marshall Space Flight Center, Huntsville, AL, 35811, USA

Abstract: Metal Matrix Composites (MMCs) are materials which consist of a metal alloy reinforced with ceramic particles or fibers. These materials possess a very high strength to weight ratio, good resistance to impact and wear, and a number of other properties which make them attractive for use in aerospace and defense applications. For example, MMCs have been extensively used for structural tubing in the space shuttle orbiter, the antenna mast of the Hubble Space Telescope, control surfaces and propulsion systems for aircraft, and tank armors. However, difficulties arise when joining those materials with fusion welding and impose limitations on the size of MMC components. Melting of the material leads to formation of an undesirable phase when molten Aluminum (Al) comes into contact and reacts with the reinforcement. This phase forms a strength depleted zone along the jointline. Friction Stir Welding (FSW) is a relatively joining technique, developed at The Welding Institute (TWI) in 1991. Because FSW occurs below the melting temperature of many metal alloys, it precludes formation of deleterious phases and results in a more favorable welded microstructure that is closer to that of the parent material. At NASA, this process was first applied to weld the super lightweight external tank for the space shuttles program. Today

*Corresponding author Tracie Prater: NASA Marshall Space Flight Center, Huntsville, AL, 35811; E-mail: tracie.prater@nasa.gov.

Yucheng Liu (Ed.)

All right reserved-© 2016 Bentham Science Publishers

FSW is employed to join structural components in Delta IV, Atlas V, and Falcon IX rockets as well as NASA's Orion Crew Exploration Vehicle and Space Launch System. Currently, FSW researchers are interested in extending the application of the process to new materials which are difficult to weld using conventional fusion techniques, such as MMCs. Rapid wear of the welding tool in FSW of MMCs is a consequence of the large discrepancy in hardness between the steel tool and the reinforcement material. This chapter summarizes the challenges encountered when joining MMCs to themselves or to other materials in structures. Specific attention is paid to the influence of the process variables for FSW on the wear process. A phenomenological model of the wear process was established based on the rotating plug model of FSW. The effectiveness of tool materials with high hardness (e.g. Tungsten Carbide, high speed steel, and tools with diamond coatings) in resisting abrasive wear is also considered. In-process force, torque, and vibration signals are analyzed to determine the feasibility of in situ monitoring of tool shape changes as a result of wear. One advantage of this model is that its successful implementation would eliminate the need for off-line evaluation of tool condition during joining. Monitoring, controlling, and reducing tool wear in FSW of MMCs are critical to full application of these materials in aerospace structures where they would be of most benefit. The work presented in this chapter can be further extended for machining of MMCs, where the wear of the tool materials is also a limiting factor.

Keywords: Advanced manufacturing, Friction Stir Welding, Materials joining, Metal Matrix Composites, Tool wear.

NOMENCLATURE

FSW	Friction Stir Welding
MMC	Metal Matrix Composite
RPM	Rotations per minute
SiC	Silicon Carbide
ℓ	Length of joint (inches)
v	Traverse rate (inches per minute)
ω	Rotation rate (rotations per minute)
W	Wear experienced by the tool during welding

D	Characteristic reinforcement particle diameter
δ	Width of the rotating plug
δ_0	Width of the rotating plug at angular position $\theta = -\pi/2$
δ_{max}	Maximum width of the rotating plug
θ	Angular position in x-y plane
P	Reinforcement fraction expressed as a percentage of workpiece volume
ΔC	Cutting arc (angular region where abrasion can occur)
ΔC_{max}	Maximum cutting arc
σ	Flow stress
t	Plunge depth
T_{total}	Total torque
Ra	Average surface roughness
Rt	Peak to valley roughness
R	Tool shoulder radius
r	Pin shoulder radius

INTRODUCTION

The reliance on ballistic techniques in launch architectures makes minimization of weight one of the most preeminent issues in spacecraft design. For any launch vehicle, cargo weights only comprise a small portion of the vehicle's weight at launch. Structural components and fuel account for the vast majority of the launch weight of a rocket. In order to improve the structural efficiency of a vehicle, the vehicle's dry weight can be reduced and the weight reduction represents a commensurate gain in cargo capacity.

Use of lighter weight materials represent one option for reducing a vehicle's weight. At present, Aluminum alloys are used as the primary aerospace structural material for fuel tanks. These alloys are lightweight, strong, well-characterized, and abundant. However, recent development of advanced materials such as composites have made it possible to further reduce the weight of the structure while satisfying (and in many cases

SUBJECT INDEX

A

- Abrasive particles 553, 554, 555
- Absorbed energy 114, 125, 127, 130, 133, 135, 144, 148
- Absorbent material vaporizes 305, 332
- Acoustic emission (AE) 357, 477
- Adhesive joints 154, 155, 160, 161, 165, 170
- Adhesive layer 159, 160, 163, 164, 166, 170, 173, 174, 175, 177, 182, 183, 184, 188, 190, 191, 193, 195, 198, 199, 201, 205, 207, 212, 213, 216, 219, 220, 222, 223, 225, 228, 229, 230, 231, 232
 - thin 166, 175, 177, 191
- Adhesive layer thicknesses 155, 160, 164, 166, 170, 198, 199, 205, 206, 208, 216, 220, 223, 229, 231
- Adhesive material 154, 155, 160, 163, 164, 165, 170, 181, 196, 200, 208, 209, 223
- Adhesive thicknesses 155, 160, 164, 173, 183, 185, 190, 194, 195, 196, 197, 198, 199, 200, 202, 204, 205, 206, 207, 209, 214, 215, 216, 217, 218, 219, 220, 221, 222, 223, 224, 225, 227, 228, 229, 230, 231, 232
 - effects of 154, 160, 163, 164, 165, 196, 208
- Aerodynamic coefficients 25
- Aerodynamic derivatives 26, 27, 395, 422
- Aerodynamic forces 13, 66, 67, 72, 74, 77, 92, 107, 110, 421, 422
- Aerodynamic lift 9, 13, 24
- Aerodynamic loads 3, 5, 6, 7, 9, 41
 - unsteady 3, 6, 9
- Aerodynamic models 7, 23
- Aerodynamic nonlinearities 7, 70
- Aerodynamics 7, 68, 70, 298, 398, 414, 415, 416, 417, 420, 424
- Aerodynamic study 67
- Aeroelastic analysis 6, 7, 25, 26, 29, 32
- Aeroelastic behavior 3, 7, 29, 36, 41, 56
- Aeroelasticity 4, 7
- Aeroelastic model 3, 26, 34
- Aeroelastic problem 5, 7, 9
- Aeroelastic stability 8, 29, 31, 52
- Aeroelastic stability boundaries 3
- Aerospace designers 443, 449, 451, 452, 455, 463
- Aerospace hydraulic systems 116
- Aerospace industry 303, 307, 355, 356, 387, 445, 446, 469, 470, 475, 483, 484, 486, 498, 500, 501, 502, 504
- Aerospace materials 451, 463, 464, 469, 486, 505
- Aerospace nanotechnology 469
- Aerothermoelastic problems 6
- AFP technology 518
- AH-1W Helicopter 288
- Aircraft 66, 67, 70, 76, 307, 311, 397, 406, 414, 415, 416, 417, 418, 421, 423, 426, 443, 444, 445, 446, 447, 448, 449, 450, 451, 452, 455, 457, 458, 459, 461, 469, 470, 473, 476, 477, 479, 481, 484, 485, 486, 499, 502, 503, 504, 505, 543
 - military 446, 458, 459, 470, 479, 484, 485
- Aircraft design, advanced 451
- Aircraft designer 449
- Aircraft engines 241

- Aircraft flight period 107
Aircraft icing mitigation 469, 475
Aircraft materials 67, 449
Aircraft structures 68, 448, 450, 451, 531
Aircraft wing model 66, 70, 86, 89, 110
Airfoil model 70, 71, 100
Airfoil model's 101
Airfoil response 108
Airfoil system 68, 71, 72, 104, 107
Alloy(s), aluminum (AA) 278, 289, 355, 375, 376, 430, 431, 443, 445, 446, 450, 451, 453, 454, 455, 456, 463, 545, 547, 561
Alloys 243, 244, 358, 443, 445, 446, 451, 452, 453, 454, 455, 456, 458, 461, 462, 463, 464, 543, 545, 547, 560, 561
metal 543, 547
titanium 443, 445, 446, 451, 454, 461, 463
unreinforced aluminum 561
Analytical stress-strain model 327
Aspect ratio 23, 471, 472, 517, 527, 529
Astronautics 470, 482, 487
Automated fiber placement (AFP) 516, 517, 518
Average adhesive thickness 184, 185
- B**
- Back-wall signals 366, 367, 368
Based adherends of specimens 184, 185
Bending control parameters 245, 246, 248, 249
Bending deformation 245, 248, 250, 251, 252
Bending loads 216, 531, 532
Bifurcating behaviors 21
Bifurcation theory 21
Bifurcation types 21
Blade chord 399, 401, 409
Blade inlet angle 246, 248
Blade selection 405, 409, 410
Bonded joints 154, 155, 157, 159, 160, 161, 165, 166, 177, 178, 192, 207, 211, 219, 230, 231
Bonded steel 189, 219, 220, 225, 226, 227
Boundary conditions 7, 88, 175, 244, 254, 257, 258, 262
Boundary values 259
Brittle materials 157
Broad frequency spectrum 22
Buckling 449, 516, 517, 519, 520, 521, 522, 525, 531
bending-induced 520, 522, 525, 531
Buckling capacity 520, 521, 523, 524, 525, 532, 533, 534, 536
Buckling load 519, 520, 523, 530, 532, 533, 536
Buckling mode shapes 525, 534, 535
Buckling performance 516, 519, 520, 527, 530, 531, 532, 533, 534, 536
- C**
- CAD model 99, 248, 249, 251, 252, 255, 257
Camera, high resolution CCD 189, 193, 194, 204, 212
Carbon-fiber reinforced polymer (CFRP) 446, 455, 457, 458, 463, 464, 499, 500

- Carbon fibers 459, 498, 500, 504, 507, 509, 510, 511
- Carbon nanotube paper 476
- Carbon nanotubes 469, 470, 471, 472, 475, 481, 482
- Card, internal pressure curve 120
- Casting-die profile 241
- Catastrophic failures 157
- Chaff/Flare dispenser bracket 280, 288, 291, 292
- Chaotic response 8, 39, 41, 42, 52
- Chaotic systems 22
- Chaotic vibrations 8, 22
- Chord length 72, 88, 250, 251
- Circumferential Location 535
- CNT implementation 483, 484, 485
- CNTs in aerospace applications 474, 487
- Cohesive fracture 157, 190, 191
- Cohesive laws 154, 155, 160, 165, 171, 174, 198, 204, 215, 218, 229
- Cohesive strength 155, 160, 230
- Cohesive zone models (CZMs) 154, 155, 159, 160, 161, 165, 173
- Collapse mechanism 115
- Commercial aircraft 475, 484, 485, 500, 504, 505
- Components 155, 241, 243, 271, 286, 303, 305, 307, 308, 310, 314, 315, 316, 320, 322, 324, 329, 330, 344, 345, 358, 369, 411, 416, 421, 422, 429, 432, 435, 436, 437, 450, 478, 501, 502, 504, 512, 513, 546
- metal 501, 502, 513
- treated 344, 345
- Composite cylinders 516, 517, 520, 522, 523, 524, 525, 527, 530, 532, 533, 534, 535, 536
- Composite materials 446, 454, 470, 474, 477, 485, 499, 501, 516, 518, 534, 546
- Composite structures 517, 518
- Compression process 503, 507
- Compressive residual stress (CRS) 303, 304, 309, 311, 315, 320, 322, 327, 330, 331, 336, 342, 343, 348, 351
- Computed radiography (CR) 357, 422
- Computer-aided design (CAD) 265, 429
- Computer modeling and simulation 115, 271
- Constant model, piece-wise 521, 522
- Constant stiffness (CS) 12, 517, 519, 520, 534, 535, 536
- Constitutive models 327, 332, 339
- Control command system 405
- Controllers, designing 415, 416
- Conventional ultrasonic 357, 362, 364, 365
- Coordinate value, optimized 249
- Cowper-Symonds relation 118
- Crack growth 157, 161
- Crack initiation 201, 202, 204, 215, 304, 308, 330
- Crack propagation 160, 163, 198, 202, 215, 218, 225, 228, 229, 231, 315, 445, 450
- Crack tip 157, 158, 159, 162, 163, 172, 173, 175, 176, 177, 178, 179, 180, 181, 188, 190, 192, 193, 201, 210, 211, 212

section of 175, 177, 178, 179
Crack tip area 222, 228
Crack tip separation 194, 195, 212, 229, 231
 local 195, 212, 229, 231
Crack tip slip, local 202, 203, 214
Crew exploration vehicle (CEV) 544, 546
Criticality number 396, 436, 438
CT subsonic aircrafts 445
Cumulatively uni-axial testing 270

D

Damping 28, 34, 35, 36, 48, 49, 57
 aeroelastic 28, 35, 36, 48, 49, 57
Damping ratios 56, 66, 73, 75, 89, 90, 91, 105, 107, 110
Darker densities 384, 385
DCB specimens 175, 176, 183, 184, 187, 188, 190, 229
Deformation 116, 125, 126, 135, 159, 203, 213, 241, 242, 245, 248, 254, 255, 261, 296
 torsional 241, 245, 248
Deformation error 265
Deformed configuration of FEA model 121, 122
Degrees-of-freedom model 78, 79, 80, 81, 82, 83, 84, 85, 104, 110
Dense periodic orbits 22, 23
Design 394, 398, 401, 404, 429, 450
 conceptual 394, 398, 401
 detailed 394, 398, 404, 429
 preliminary 429

 safe 450
Design equation 449
Design experiments method 395
Design optimization 516, 523, 524, 531, 532
 multi-objective 531, 532
Design parameters 401, 404, 415, 416
Design process 135, 405, 415, 450, 531
Design relationships 443, 448, 449
Double cantilever beam (DCB) 163, 164, 174, 175, 182, 190, 229
Ductile materials 157, 159
Dynamical systems 20, 21, 22, 421
Dynamic model, structural 71
Dynamic modeling 395, 415, 421
Dynamic response 8, 41, 45, 48, 57, 70, 71, 270
Dynamics 67, 281, 299, 414, 415, 416, 421, 422, 428
 structural coupling 67
Dynamic structural response 72

E

Eddy current testing 357, 358
Elastic displacements 4, 10
Elastic fins 7, 9, 32, 34, 35, 36
Elastic rotations 5
Electrical engines 405
Electromagnetic particles 273
Elements, piezoelectric 359, 364, 369
Elliptical cylinders 520, 533, 534, 535, 536

- End notched flexure (ENF) 161, 163, 164, 175, 177, 182, 229, 230
- Energy release rate (ERR) 157, 158, 193, 195, 203, 211, 212, 214
- Energy release rate component JI 180, 181
- ENF specimen 178, 186, 189, 201, 206
- Engine and fuel system 395, 405
- Engine gears 411, 412
- Engine group 430
- Engines 241, 395, 405, 406, 407, 408, 411, 414, 429, 431, 438, 446
- electric 405, 406, 407, 408
 - piston 405, 406, 407, 408
 - turbine 405, 407
- Equations 3, 10, 21, 89, 169, 170, 423, 424, 426
- characteristic 21, 423, 424, 426
 - governing 3, 10, 89, 169, 170
- Estimated forces 78, 82, 92, 93, 94, 95, 96, 97, 98, 110
- Estimated forces and moments 78, 82, 92, 96, 110
- Excitation system 71
- Expansion waves 15, 16, 17
- Explicit FEA solver 116
- F**
- Failure mode effect analysis (FMEA) 435
- Fatigue analysis 271, 280, 281, 290, 291, 292, 296, 298, 300, 311, 322, 344
- Fatigue failures 271, 298, 304, 309, 327, 346
- Fatigue life prediction 308, 309, 310, 313
- Fatigue loading 309, 314, 315, 349
- Fatigue prediction methods 313
- Fatigue strength 278, 304, 314, 445, 446
- Fatigue tests 270, 271, 281, 291, 296, 299, 432
- FEA models 116, 118, 119, 120, 121, 122, 125, 149, 316, 336
- FEA software 287
- Fiber, glass 169, 504, 507, 509, 510, 511
- Fiber content 502, 506, 507, 508, 509, 510
- Fiber orientation angle 517, 521
- Fiber-reinforced polymer composite (FRPC) 517
- Fiber reinforcements 500, 501, 502, 509, 512
- continuous 509, 512
 - continuous carbon 500, 501, 502
- Fighter aircraft loading standard for fatigue (FALSTAFF) 310
- Finite element analysis (FEA) 114, 122, 124, 135, 138, 139, 145, 150, 160, 244, 270, 276, 311, 327, 331, 523, 524
- Finite element model 34, 66, 68, 70, 299, 336, 338, 521
- Flap and plunge direction 39, 40, 41, 43, 44, 46, 47, 50, 51, 54, 55
- Flapping motions 9, 418
- Flexural strength 502, 505, 506, 507, 508, 509
- Flight missions 406, 407, 408
- Flight regimes 408, 418

- Flight tests 271, 274, 278, 288, 289, 290, 432, 434
- Flow, supersonic 11, 15, 16, 27
- Flow properties 6, 15, 18
- Flutter divergence 30, 31, 32
- Force determination error 93, 94, 95, 97, 98, 99
- Force determination methods 66, 68, 75, 77, 78, 86, 92, 110
- Forces 4, 10, 13, 14, 66, 72, 74, 76, 77, 78, 82, 83, 92, 94, 96, 99, 101, 107, 114, 126, 139, 190, 201, 210, 229, 230, 231, 349, 358, 396, 417, 420, 422, 424
- actual 66, 74, 107
- critical 229, 230, 231
- excitation 72, 74, 78, 101, 107
- generalized 4, 10
- Forward flight 398, 404, 405, 416, 417, 418, 423, 426, 427, 428
- Fracture, basic modes of 156
- Fracture energy 159, 160, 163, 164, 173, 192, 207, 211, 219, 225, 230
- Fracture energy JIIC 202, 215, 218, 219, 20, 221, 224
- estimated 218, 220, 221, 224
- Fracture process 158, 160, 165
- Fracture strength 229, 230, 231, 232
- Fracture tests 155, 173, 174, 187
- Fracture toughness JIC 229, 231, 232
- Free-play 3, 4, 5, 8, 9, 11, 13, 14, 36, 37, 56, 57
- Free-stream surface 18
- Frequency domain 69, 70, 73, 89, 108, 276, 281, 299
- Frequency domain methods 281, 282
- Frequency response functions (FRFs) 66, 77, 78, 82, 92, 99, 101, 104, 107, 108
- Frequency response matrix 74, 75, 76, 77, 99
- Frequency separation 413
- Friction stir (FS) 370, 376, 377, 378, 385, 386, 387, 556
- Friction-stir-welding (FSW) 355, 376, 543, 544, 546, 547, 549, 553, 556, 558, 559, 561
- FRPC materials 517
- FSW, application of 547
- FSW of MMCs 548, 549, 552, 553, 554, 557, 558, 561
- FSW process 546
- Fuel consumption 407, 475, 476
- Fuel systems 395, 405
- Functional composite components 500
- G**
- Gear ratio 408, 410, 411, 412, 413
- Geometrical parameters 3, 29, 36
- Geometric characteristics 401, 402, 438
- Geometries 11, 15, 27, 29, 33, 160, 163, 184, 185, 196, 261, 271, 293, 299, 308, 311, 316, 337, 342, 347, 358, 450, 513
- concave 316, 342
- curved 308, 347
- Ground vibration test (GVT) 71, 75, 76, 101, 102, 108, 110

Group 184, 185, 190, 191, 192, 193, 164, 195, 196, 198, 200, 201, 202, 203, 204, 205, 207, 210, 216, 217, 218, 429, 499, 547, 552
specimen in 190, 191, 192, 194, 201, 202, 204

H

Helicoids hole 100
Helicopter components 271, 272
High-temperature CFRP 458
Hinge frictional torque 3, 56
Hovering flight 408, 409, 417, 418, 423, 424, 426
H Plunging displacement 4
Hugoniot elastic limit (HEL) 318, 328, 335, 336, 341
Hydraulic system of aerospace 115, 150
Hydrophobicity 469

I

Impact 118, 119, 133, 134, 145, 150, 329, 543, 556, 561
mid-position 133, 134, 150
quarter-position 133, 134, 150
Impact behavior 116, 117, 149, 511
Impact energy 117, 134, 135, 145
Impact force 125, 126, 135
Impact forces, higher 134, 145
Impact hammer 101, 102, 103
Impact positions 114, 116, 125, 127, 128, 129, 130, 133, 145, 150
Impact resistance 134, 145, 149, 181

Impact response 116, 133, 135, , 142, 145, 150
lateral 116, 142, 145, 150
Impact simulations 119, 120, 122
Impact strength 505, 506, 507, 509, 511
Impulse response functions (IRFs) 104
Inclinometer 188, 191, 211
Index offset 373, 374, 388
Industry, modern 135, 154, 155
Initial angle of attack 3, 24, 25, 26, 27, 29, 35, 45
Initial crack 186, 194, 204
Initial crack length 184, 185, 210, 211, 212, 214, 215, 217, 222, 223, 224, 225, 227, 228, 231, 232
Initial crack tip 157, 192, 193, 194, 202, 204, 211, 212, 214, 222, 229
Initial crack tip length 222, 228
Integration process 270, 274, 280
Integrity, structural 355, 356, 475
Interfacial strength 155, 173, 198, 200, 207, 209, 218, 219, 225, 229, 231
Interfacial strength σ_{max} 198, 200, 218, 225, 227
Interfacial traction-separation laws 154, 160, 161, 164, 173, 198, 209, 225
Interfacial traction-separation laws of bonded steel 219, 225, 226
Interlayer, adhesive 158, 163, 164
Internal defect 377, 378, 385, 386
Internal pressure 114, 115, 116, 117, 119, 120, 125, 127, 131, 133, 134, 135, 139, 142, 145, 149, 150
effects of 114, 116, 131, 142
influence of 116, 117, 133, 142
Inverse deformation 242

- Investment casting 241, 242, 243, 251, 255, 264
- Isotropic fibre distribution 499
- L**
- Lack of penetration (LOP) 382, 383
- Lagrangian dynamics 9
- Laser peening process 311, 314, 316, 324, 332, 333, 334, 339, 340, 341
- Lateral motion 423, 424, 425, 426
- Lateral wave (LW) 366, 367, 368
- Laws of bonded steel 220, 226, 227
- Least squares complex exponential (LSCE) 103, 104
- Length of welds 548, 552, 555, 558
- Lightweight materials 498, 545
- Limit cycle oscillations (LCOs) 8, 20, 22, 38, 48, 52, 57, 71
- Linear elastic fracture mechanics (LEFM) 157, 158, 159, 161
- Liquid penetrant testing 357
- Loading conditions 119, 120, 165, 271, 313, 351, 443, 448, 449
- Loading force, critical 229, 230, 231
- Loading modes 161, 162
- Loadline displacements 191, 192, 193, 194, 201, 202, 210, 211
- Local maxima 37, 38, 57
- Local piston theory 4, 24, 25, 29
- Local tests 154, 160, 163, 164
limited 154
- Longitudinal modes 423, 424, 426, 427
- Longitudinal wave 359, 360, 366
- Low cycle fatigue 327, 332, 346
- LS-DYNA 114, 115, 116, 119, 120
- Lyapunov exponent(s) 20, 22, 23, 38, 39, 41, 42, 49, 52, 53
- M**
- Magnetic particle testing 357
- Material behavior 308, 334
- Material combinations 504, 507, 508, 509, 510, 511, 513
- Material nonlinearities 7, 114
- Material parameters 314, 346, 359
- Material properties 33, 118, 119, 254, 289, 316, 371, 463, 523, 534, 548, 554, 561
- Materials 100, 116, 155, 156, 157, 159, 160, 170, 181, 271, 275, 299, 305, 306, 312, 316, 318, 320, 327, 329, 330, 331, 332, 333, 334, 335, 336, 338, 339, 340, 341, 343, 344, 346, 347, 351, 358, 359, 360, 361, 362, 366, 369, 371, 375, 443, 444, 448, 449, 450, 451, 458, 461, 462, 463, 464, 469, 470, 471, 473, 475, 480, 484, 485, 486, 500, 501, 504, 508, 513, 517, 534, 543, 544, 546, 547, 548, 549, 554, 555, 557, 558, 561, 562
peened 305, 312, 331
plasticized 546, 548
reinforcement 504, 544, 547, 561
- Materials parameters 229, 230, 231
- Materials selection 443, 450, 452
- Material stirring 547, 548, 549
- Material surface 306, 308, 339
- Mathematical model 414, 415, 417
- Maximum buckling capacity 521, 526, 531
- Maximum deformation 127, 129, 261
- Maximum deformation of pipeline models struck 132

- Maximum fatigue life 303, 308, 309, 318, 319, 324
- Maximum impact force 127, 128, 133, 134, 142, 145, 146, 149, 150
- Maximum Lyapunov exponent 22, 23
- Maximum transverse displacement 134, 150
- Mean time between failures (MTBF) 395, 435
- Mean time to failure (MTTF) 395, 435
- Measurement locations 273, 276, 278, 279
- Metal fatigue 270
- Metal matrix composites (MMCs) 543, 544, 547, 548, 549, 552, 553, 554, 557, 558, 559, 561
- Metamodeling based design optimization (MBDO) 516, 520, 536
- Method of die-cavity 241
- Microchips to large aircrafts 155
- Mid-span duration 316, 317, 320
- Mid-span impact 138, 140, 142, 143, 144, 145, 146, 147, 148, 149
- Mild-steel pipelines 135
- Military aircraft wings 461, 462, 463
- Military standards 270, 288, 294
- Model 3, 7, 11, 28, 29, 32, 66, 70, 71, 87, 99, 100, 101, 103, 104, 110, 118, 120, 126, 127, 160, 161, 242, 255, 274, 275, 286, 293, 312, 313, 316, 327, 336, 338, 341, 346, 409, 414, 415, 416, 417, 421, 422, 431, 544, 551, 553, 554, 555, 557, 562
- cowling 274, 275
- empirical 312, 331, 561
- Modeling 5, 9, 137, 160, 274, 318, 327, 337, 347, 405, 415, 480, 520
- Modern toughened adhesives 157
- Mode shapes 4, 5, 10, 34, 66, 89, 90, 107, 110, 275, 299
- natural 4, 5, 10, 34
- second 89, 90
- Molten aluminum 543, 547
- Monte carlo method 286
- Morozov's discrepancy principle 69
- Multi-axial testing 271, 281
- Multi-degree-of-freedom model 70, 88, 92, 93, 94, 95, 96, 97, 98, 99, 110
- Multiple-degree-of-freedom system 66
- Multiple regression model (MRM) 551, 552
- N**
- Nanomaterials 474, 485
- Nanotube diameter 471, 472
- National aeronautics and space administration (NASA) 474, 476, 543, 546, 548
- NDE techniques 355, 356, 357, 358
- Non-destructive evaluations 356
- Non-linear aeroelastic behavior 3
- Nonlinear dynamical systems 20
- Non-periodic responses 22
- Numerical models 155, 160, 161, 287, 327, 350
- Numerical simulations 114, 149, 242, 252, 255, 263, 266, 346

O

Ohio supercomputing center (OSC) 338
Operational flight tests 274, 278
Optimum design 135, 255, 395, 524
Orientation angles 518, 519, 521, 522, 526, 535
Oscillations 23, 39, 46, 52, 359, 424, 425, 427

P

Parameterization studies 548
Parvan 395, 398, 399, 400, 401, 404, 405, 407, 408, 412, 418, 419, 422, 423, 424, 425, 426, 428, 429, 431, 433, 434, 436, 437, 438
 components of 436, 437
Parvan components dimensions 402, 403
PAUT system 371, 372, 386, 388
Peel strength 228
Peened components 303, 308, 309, 313, 318, 329, 330, 332, 344
Phased array ultrasonic testing (PAUT) 355, 356, 357, 362, 363, 369, 372, 373, 375, 376, 377, 385, 386
Phase plane diagram and time histories 39, 40, 41, 43, 44, 46, 47, 50, 51, 54, 55, 59, 60, 61, 62
Phthalonitrile resin system 459, 460
Pipeline models struck 127, 131, 132, 133
Pipeline's impact force 116
Piston theory 3, 4, 6, 9, 14, 15, 23, 24, 25, 29
 local 4, 24, 25, 29

Plasma 305, 306, 332, 333
Plastic deformation 159, 164, 190, 201, 297, 298, 306, 318, 333, 336, 338
Plastic dissipations 160, 162, 170, 190, 192, 196, 202, 211, 215, 220
Plasticity mechanisms 117, 150
Plastics, reinforced 498, 499, 500
Plastic strain 163, 335, 336, 339
Plies 517, 518, 521, 522, 526, 528, 530, 531, 535
 steered 517, 526, 530, 531
Plies candidate 520, 522, 530
Plug, rotating 545, 553, 554, 557
Plug model, rotating 544, 553, 554, 556, 557, 559
Plunge direction 39, 40, 41, 43, 44, 46, 47, 50, 51, 54, 55
Polyimides 459, 463, 464, 483
Power Spectral Density (PSD) 276, 277, 281, 282, 283, 284, 285, 288, 289
Power transmission system 395, 408, 410
Prandtl-Meyer theory 16
Precautions, recovery 436, 437, 439
Preferred system concept (PSC) 476
Pressure pulse 306, 332, 333, 334, 337, 340
Pressurized pipelines 114, 115, 116, 117, 119, 120, 121, 122, 133, 145, 149, 150
Probability Density Function (PDF) 281, 284, 285, 286, 287, 289, 395
Problem, axial fatigue 332, 346, 350, 351

Procedure, modified explicit 338
Process, random 282, 285
PSD function 282, 283, 285
PSD matrix 289
Pseudo-inverse method 78, 92, 99, 110

Q

QI designs 529, 530, 531
Quartic polynomial functions 138
Quarter span impact 141, 142, 143, 144, 145, 146, 147, 148, 149
Quartic response surfaces 140, 141
Quasi-isotropic (QI) 519, 525, 526, 527, 528, 529, 533, 534, 535, 536

R

Radar cross section (RCS) 479
Radiographic testing (RT) 356, 357, 358, 378, 379, 385, 386
Radiography 355, 357, 378
Rayleigh dissipation function 4, 10, 11
Regions, antenna integration 274, 275
Reinforcement particles 547, 555, 557, 558
Relative rotation angle 223, 228
Relaxation behavior 331, 332, 345, 350
Relaxation effect 309, 312, 327, 331, 332, 345, 346, 349, 351
Relaxation models 317, 322, 323
Response functions 78, 92, 136, 139
Response surface method (RSM) 135, 136, 138
Response surfaces 114, 127, 133

Reverse design methodology 241, 242
Root mean square (RMS) 286
Root mean square error (RMSE) 137, 139
Rotational, estimated 79, 81, 83, 84, 85, 93, 95, 96, 97, 98
Rotational speeds 410, 411, 432, 433
Rotorcraft 469, 475, 480, 484, 485
Rotor diameter 399, 402, 403

S

Sea level (SL) 34, 36, 56, 399
Secondary Hopf 21
Shape form error 242, 265
Shear strength 209, 220, 221, 460
Sheet metal model 296
Sheet molding compound 498, 499, 500, 501, 502, 505, 507, 508, 509, 510, 512, 513
Sheet molding compound formulations 508, 509, 510, 512
Sheet molding compound materials 512
Sheet molding compounds 499, 501, 509, 512
Shock and expansion analysis 4
Shock waves 7, 306, 312, 332, 333, 334, 335, 337, 338, 339, 340
Shrinkage factors (SFs) 244
Simulation models 308, 310, 351
Simulation process 257, 258, 261
Skin temperature 452, 457, 459
SLB specimen 178, 179, 180, 181, 186
Small-scale turbofan engines 405
Solidification 241, 243, 244, 255
Sorted k-fold approach (SKA) 309, 320, 324

- Sound waves 359, 360, 361, 369, 370, 371, 372, 375
 high frequency 369, 370
- Space elevator 469, 482
- Specimens 160, 162, 172, 175, 177, 178, 182, 183, 184, 185, 190, 195, 196, 198, 209, 210, 211, 212, 214, 215, 216, 218, 229, 230, 231, 281, 331, 339, 340, 347, 372, 378, 381, 508
 effective 185, 190
 five 195, 196, 198
 five groups of 184, 185
 groups of 183, 184, 185, 190
- SST aircrafts 446, 455, 458, 459
- Stability derivatives 416, 420, 424
- Stacking sequence 410, 525, 530, 533, 535
- Stagger angle of CAD model 248
- Static mass moment 5, 12
- Steel adherends 164, 209, 212
- 3-D simulation 395
- Strain rate effects 118, 335, 339
- Strain rates 118, 328, 339
- Stress 115, 156, 176, 177, 179, 181, 261, 304, 318, 320, 330, 331, 348
 normal 176, 177, 179, 181
 tensile 115, 156, 261, 304, 318, 320, 330, 331, 348
- Stress corrosion cracking (SCC) 444, 448
- Stress field, residual 316, 338, 345, 347
- Stress intensity factor (SIF) 157, 444, 450
- Stress range 285, 286
- Stress relaxation 308, 344, 345, 346, 347, 348, 350
- Stress relaxation model 316, 327
- Stress spectrum 311, 314, 316
- Stress-strain behavior 332, 346, 347
- Stress values 277, 278, 286, 299, 300
- Structural components 303, 304, 308, 309, 316, 323, 324, 330, 344, 448, 450, 451, 463, 464, 503, 517, 518, 544
- Structural improvement 519, 520, 530
- Structural materials 445, 447, 454, 464, 545, 548
- Structural member 444, 449
- Structural model 3, 7, 9, 29, 71
- Structural nonlinearities 7, 8, 70, 300
- Structural performance 516, 517, 519
- Structural responses 66, 67, 74, 75, 270, 523
- Structures, bonded 154, 156, 165
- Subsonic aircrafts 445, 452, 453, 454
- Subsonic aircraft's structures 452, 453, 454
- Subsonic structures 445, 452
- Supersonic aerodynamic characteristics 6
- Supersonic cruise conditions 447
- Supersonic fins 7, 29, 31, 52
- Supersonic flight 451, 462, 463
- Supersonic/hypersonic flow 5
- Supersonic regime 6
- Surface enhancement methods 333, 344
- Surface enhancement techniques 304, 308, 329, 330
- T**
- Tail rotor diameter 399, 401, 403
- TCG calibration 374, 388

- Techniques 6, 115, 136, 162, 356, 357, 373, 381, 386, 387, 416, 431, 549, 556, 557, 560, 561
 traditional inverse 79, 93
Temperature effects 306, 339, 341
Temperature resistance 458, 459, 461
Tensile modulus 507, 509, 510
Tensile strength 181, 200, 458, 460, 472, 502, 505, 506, 507, 508, 509, 510, 511
Tests, wind tunnel 26, 68, 71, 99, 107, 108, 110, 432
Test specimens 161, 187, 188, 359, 508
Theoretical model 8, 134, 165
Theory, classical beam 165, 166, 167
Thermal conductivity 470, 471, 472
Thick fins 3, 6, 15, 16, 32
Thick supersonic fin 4, 6, 9, 36, 57
Ti-6Al-4V material 327, 340
Time-corrected-gain (TCG) 374
Time derivatives 37, 56
Time-of-flight-diffraction 362, 366, 368
Time of flight diffraction (TOFD) 357, 362, 363, 366, 368
Time series, torsional angle 37, 41
Titanium 445, 446, 457, 471, 505, 547
Tool materials 544, 548, 558, 559, 561
Tool probe 549, 555, 556
Tool surface 554, 555, 557
Tool wear 544, 552, 556, 561
Torque 396, 408, 410, 411, 428, 544, 559, 561
Torsional control parameters 245, 248
Torsional shear stresses 444, 449
Traction-separation 229, 230, 231
Traction-separation laws 154, 161, 163, 164, 194, 198, 199, 202, 212, 213, 214
 equivalent interfacial 163, 194, 198, 199, 202, 212, 213, 214
 local interfacial 154, 161, 163, 164
Traditional pseudo-inverse technique 77, 92
Traffic monitoring 397, 398, 400, 401, 438
Translational force 80, 82, 84, 85, 94, 95, 97, 98
Transmission system design 411, 412, 413
Transmitting system 405, 408, 411, 413
Transverse deformations 18
Transverse displacements 133, 150
Truncated singular value decomposition (TSVD) 69
Turbine blade 241, 242, 243, 245, 249, 252, 254, 255, 261, 262, 264, 265, 308
Two degree-of-freedom pitch-plunge system 72
Two-step optimization strategy 303, 309, 319
- U**
- Ultimate tensile strength (UTS) 444, 455, 460
Ultrasonic testing (UT) 357, 358, 362, 364
Uni-axial fatigue testing error 271
Unmanned aerial vehicles (UAVs) 395, 397, 405, 414, 469, 470, 480, 481, 482

Unsteady aerodynamic loading models
5

V

Vibration analysis 274, 276, 278
Vibration fatigue analysis 283, 285,
288, 289
Vibration fatigue method 282, 287, 298,
299
Vibration levels 274, 278, 280

W

Weight saving 476, 483, 519
Weight sizing 399, 438
Weld defects 355, 356, 357
Weld image 382, 383, 384, 385
Welding defects 356, 357, 369, 376,
382
The welding institute (TWI) 543, 546
Wing model 71, 87, 99, 100, 101, 102,
110

X

X-ray images 381, 385, 386
X-ray radiography 355, 385, 386, 387

Z

Zone 155, 157, 158, 163, 165, 171, 202,
215
cohesive 158, 165, 171
failure process 165
plastic 155, 157, 158, 163, 202, 215



Yucheng Liu

Dr. Yucheng Liu is Associate Professor at the Department of Mechanical Engineering at Mississippi State University. Prior to joining Mississippi State University, Dr. Liu was an Assistant Professor of Mechanical Engineering at the University of Louisiana at Lafayette from 2009 to 2014. Dr. Liu received his Master and PhD degrees in Mechanical Engineering from the University of Louisville and his Bachelor degree from Hefei University of Technology. Dr. Liu's wide research interests include multiscale modeling and simulation, high strain rate deformation and failure analysis, mechanics and science of materials, marine and hydrokinetic technology, etc. To date, Dr. Liu has authored and coauthored about 150 peer reviewed publications, including 12 books/chapters, 79 journal articles, and 59 conference proceedings. He has also led or been an important personnel in many research projects with total grant funding of \$3.6 million. Given world reputation and expertise in his areas, Dr. Liu has reviewed proposals for US Department of Defense, US Department of Energy, and US National Science Foundation. He has also edited and reviewed over 50 peer reviewed journals and provided organizing, chairing, and reviewing services to more than 15 international conferences. Dr. Liu is a Professional Engineer registered in Ohio and holds active membership in American Association for the Advancement of Science American Society of Mechanical Engineers (ASME), Society of Automotive Engineers (SAE), and American Society of Engineering Education (ASEE).